https://doi.org/10.5194/egusphere-2024-654
Preprint. Discussion started: 3 April 2024

Diurnal, seasonal, and interannual variations in $\delta(^{18}O)$ of atmospheric O_2 and its application to evaluate changes in oxygen, carbon, and water cycles

Shigeyuki Ishidoya[1], Satoshi Sugawara[2], Atsushi Okazaki[3]

[1]National Institute of Advanced Industrial Science and Technology (AIST), Tsukuba 305-8569, Japan
[2]Miyagi University of Education, Sendai 980-0845, Japan
[3]Chiba University, Chiba 263-8522, Japan

Correspondence to: Shigeyuki Ishidoya (s-ishidoya@aist.go.jp)

Abstract.

Variations in the $\delta(^{18}O)$ of atmospheric O_2, $\delta_{atm}(^{18}O)$, is an indicator of biological and water processes associated with the Dole-Morita effect (DME). The DME and its variations have been observed in ice cores for paleoclimate studies, however, variations in present-day's $\delta_{atm}(^{18}O)$ have never been detected so far. Here, we present diurnal, seasonal, and interannual variations of $\delta_{atm}(^{18}O)$ based on observations at a surface site in central Japan. The average diurnal $\delta_{atm}(^{18}O)$ cycle reached a minimum during the daytime, and its amplitude was larger in summer than in winter. We found that use of $\delta_{atm}(^{18}O)$ enabled separation of variations of atmospheric $\delta(O_2/N_2)$ into contributions from biological activities and fossil fuel combustion. The average seasonal $\delta_{atm}(^{18}O)$ cycle reached at a minimum in summer, and the peak-to-peak amplitude was about 2 per meg. A box model that incorporated biological and water processes reproduced the general characteristics of the observed diurnal and seasonal cycles. A slight but significant secular increase of $\delta_{atm}(^{18}O)$ by (0.22 ± 0.14) per meg a^{-1} occurred during 2013–2022. The box model could reproduce the secular trend if consideration was given to long-term changes of terrestrial gross primary production (GPP), photorespiration, and $\delta(^{18}O)$ of leaf water ($\delta_{LW}(^{18}O)$). We calculated changes of $\delta_{LW}(^{18}O)$ using a state-of-the-art, three-dimensional model, MIROC5-iso. A comparison between the observed and simulated $\delta_{atm}(^{18}O)$ values suggested that there had been a recent increase of global GPP, a slight decrease of photorespiration, and an increase of carboxylation (total carbon fixation).

https://doi.org/10.5194/egusphere-2024-654
Preprint. Discussion started: 3 April 2024

1 Introduction

The $^{18}O/^{16}O$ ratio of atmospheric O_2, $\delta_{atm}(^{18}O)$, is higher by about 24 ‰ Vienna-Standard Mean Ocean Water (V-SMOW) (e.g. Craig, 1961; Barkan and Luz, 2005) than that of ocean water (0 ‰) because of various processes in the global oxygen and water cycles. The enrichment of $\delta_{atm}(^{18}O)$ is well known as the Dole-Morita effect (DME) (Dole, 1935; Morita, 1935). The DME is determined from the balance between enrichment of $\delta_{atm}(^{18}O)$ due to discrimination against ^{18}O during terrestrial/marine respiratory O_2 consumption and the terrestrial/marine photosynthetic O_2 flux, for which the $\delta(^{18}O)$ is close to that of ocean water. The isotopic effects of dark respiration, photorespiration, and the Mehler reaction associated with terrestrial respiration are 18, 21.2, and 15.3 ‰, respectively, and the terrestrial photosynthetic O_2 flux is also affected by discrimination against ^{18}O during evapotranspiration (4.4 ‰). (See Table 1 of Bender et al. (1994) for a summary of the isotopic effects related to the DME.) The DME is a useful tool for examining Earth system models because it integrates land and ocean biological and climatic components (e.g., Bender et al, 1994; Hoffman et al., 2004). Some paleoclimate studies have focused on the temporal changes of $\delta_{atm}(^{18}O)$. Bender et al. (1994) have reported that the DME is on average lower by 0.05 ‰ than that of air at present, and that variations of the DME from the average are ±0.2 ‰. They have suggested that the variability is small and may be due to variations of the relative rates of primary production on the land and in the ocean. Severinghaus et al. (2009) have reported the $\delta_{atm}(^{18}O)$ in the Siple Dome ice core, Antarctica, and have found that its variations over the past 60 ka are related to Heinrich and Dansgaard-Oeschger events. They have suggested that the DME is primarily governed by the strength of the Asian and North African monsoons and have confirmed that widespread changes of low-latitude terrestrial rainfall accompany abrupt climate changes.

Hoffman et al. (2004) have developed a model of the DME by combining the results of three-dimensional (3D) models of carbon and oxygen cycles with results of atmospheric general circulation models with built-in water isotope diagnostics and have reproduced the average DME of 22.4 or 23.3 ‰. However, they did not simulate temporal or spatial variations of $\delta^{18}O_{atm}$ in the present atmosphere, which have not yet been detected. The diurnal cycle of the atmospheric O_2/N_2 ratio at forest sites is caused mainly by activities in the terrestrial biosphere, and the peak-to-peak amplitudes are roughly about 100 per meg (1 per meg is 0.001 ‰) (e.g., Ishidoya et al., 2013a; Battle et al., 2019; Faassen et al., 2023). Diurnal variations of $\delta^{18}O_{atm}$ associated with activities in the terrestrial biosphere are therefore expected to be very small. Keeling (1995) has predicted that $\delta_{atm}(^{18}O)$ should be lower in summer than in winter in both hemispheres by about 2 per meg by assuming a 100 per meg seasonal increase of the atmospheric O_2/N_2 ratio due to the input of terrestrial and oceanic photosynthetic O_2, which has a $\delta(^{18}O)$ that is lower than $\delta_{atm}(^{18}O)$ by 20 ‰. Seibt et al. (2005), who calculated potential effects of human activity on the DME, have estimated that global changes of the terrestrial biosphere may have led to a decrease of $\delta_{atm}(^{18}O)$ on the order of 70 per meg over the last 150 years (–0.5 per meg a^{-1}). They have estimated that 2/3 of the total decrease is due to a decrease of photorespiration globally accompanied by a 100 μmol mol^{-1} increase of the fraction of atmospheric CO_2 during those 150 years. Diurnal, seasonal, and

https://doi.org/10.5194/egusphere-2024-654
Preprint. Discussion started: 3 April 2024

secular changes of $\delta_{atm}(^{18}O)$ in the present atmosphere will therefore be a new indicator of activities of the land and oceanic biospheres, although sufficiently precise measurements of $\delta_{atm}(^{18}O)$ to validate the suggestions by Keeling (1995) and Seibt et al. (2005) have never been reported.

In this study, we present diurnal, seasonal, and secular changes of $\delta_{atm}(^{18}O)$ observed at Tsukuba (TKB), Japan (36° N, 140° E). We then compare the observed changes of $\delta_{atm}(^{18}O)$ at TKB with a one-box model that incorporates the biosphere and water processes associated with the DME. To evaluate the secular changes of water processes, we used an isotope-enabled version of the Model for Interdisciplinary Research on Climate (MIROC5-iso) (Okazaki and Yoshimura, 2019) and calculated the $\delta(^{18}O)$ of leaf water, $\delta_{LW}(^{18}O)$. Finally, we inferred from a comparison between the observed and simulated $\delta_{atm}(^{18}O)$ that there has been a recent secular increase of gross primary production (GPP), a decrease of photorespiration, and an increase of total carbon fixation.

2 Methods

2.1 Continuous atmospheric measurements of $\delta_{atm}(^{18}O)$ and $\delta(O_2/N_2)$

Air was sampled with a diaphragm pump from an air intake located on the roof of a laboratory building of the National Institute of Advanced Industrial Science and Technology (AIST) at TKB. The gas velocity exceeded 5 m s^{-1} (4 mm i.d. and a flow rate of 4 L min^{-1}) at the tip of the air intake, which was high enough to prevent thermally diffusive inlet fractionation (Sturm et al., 2006; Blaine et al., 2006). The sample air was introduced into a 1-L, stainless-steel buffer tank after water vapor in the air had been reduced by using an electric cooling unit at 2 °C. The gas was then exhausted from the buffer tank at a flow rate of about 4 L min^{-1}. A small portion of this exhausted gas was introduced into a 3.2-mm (1/8 in.) o.d. stainless-steel tube, and any remaining water vapor was removed using a cold trap at −90 °C. Finally, the remaining sample air was vented through an outlet path at a rate of about 10 mL min^{-1}, and a minuscule amount of it was transferred to the ion source (or waste line) of a mass spectrometer (Thermo Scientific Delta V) through a thin, insulated, fused-silica capillary. The reference air was always supplied from a high-pressure cylinder at a flow rate of about 4 mL min^{-1}, and a minuscule amount of it was introduced into the ion source (or waste line) of the mass spectrometer through another fused-silica capillary. The standard air, which was supplied from a high-pressure cylinder at a flow rate of 4 mL min^{-1}, was introduced like the reference air into the ion source (or waste line) of the mass spectrometer, but through the line for sample air. We analysed the standard air about once per two months. Details of the continuous measurement system we used have been reported by Ishidoya and Murayama (2014).

For the continuous measurements of stable isotopic ratios of O_2, N_2, and Ar ($\delta_{atm}(^{18}O)$, $\delta_{atm}(^{15}N)$, and $\delta_{atm}(^{40}Ar)$) as well as the O_2/N_2 ratio and amount fraction of CO_2, we repeatedly conducted alternate analyses of the sample and reference air. The time required to obtain a measured value was 62 s. However, the standard deviation of the $\delta_{atm}(^{18}O)$ was about 20 per meg, which

https://doi.org/10.5194/egusphere-2024-654
Preprint. Discussion started: 3 April 2024

was much larger than the standard deviation required to detect the expected respective seasonal (2 per meg) and secular changes (–0.5 per meg a^{-1}) in $\delta_{atm}(^{18}O)$ by Keeling (1995) and Seibt et al. (2005). We therefore averaged more than 1000 data and used the averaged value as the observed $\delta_{atm}(^{18}O)$. This averaging theoretically made the standard error of the observed $\delta_{atm}(^{18}O)$ less than 0.6 per meg. For this purpose, the measured values of the $\delta_{atm}(^{18}O)$ for the same air sample needed to not show any temporal drift, at least during the averaging period. In this regard, we confirmed that the measured values of the $\delta_{atm}(^{18}O)$ against reference air were stable enough for a period much longer than the averaging period. We therefore needed to calibrate with a primary and secondary air standard (described below) only once per two months. Figure 1 shows an example of the measured $\delta_{atm}(^{18}O)$ of a standard air against reference air. We found the standard deviations of 200 and 400 averaged data to be 1.4 and 0.4 per meg, respectively, which are consistent with the theoretically expected values of 1.3 and 1.0 per meg.

The $\delta_{atm}(^{18}O)$ and $\delta(O_2/N_2)$ were reported in per meg:

$$\delta_{atm}(^{18}O) = \frac{R_{sample}(^{18}O^{16}O/^{16}O^{16}O) - R_{standard}(^{18}O^{16}O/^{16}O^{16}O)}{R_{standard}(^{18}O^{16}O/^{16}O^{16}O)}, \quad (1)$$

$$\delta(O_2/N_2) = \frac{R_{sample}(^{16}O^{16}O/^{14}N^{14}N) - R_{standard}(^{16}O^{16}O/^{14}N^{14}N)}{R_{standard}(^{16}O^{16}O/^{14}N^{14}N)}. \quad (2)$$

Here, the subscript "sample" and "standard" indicate the sample air and the standard air, respectively. Because O_2 constitutes 0.2093 mol mol^{-1} of air by volume (Aoki et al., 2019), a change of 4.8 per meg of $\delta(O_2/N_2)$ is equivalent to about a change of 1 μmol mol^{-1}. In this study, the $\delta_{atm}(^{18}O)$ and $\delta(O_2/N_2)$ of each air sample were determined against our primary standard air (cylinder no. CRC00045) using a mass spectrometer. Our standards were dried ambient air or industrially purified air-based CO_2 in 48-L high-pressure aluminium cylinders. The standards were classified as either primary or secondary. Figure 2 shows the value of each analysis and the corresponding annual average of $\delta_{atm}(^{18}O)$ of three secondary standards against the primary air standard. As shown in Figure 2, variations of the annual average $\delta_{atm}(^{18}O)$ of our three secondary standards were within ±0.8 to ±1.1 per meg (±0.9 per meg, on average) and nearly stable for 10 years with respect to the primary standard. We therefore allowed an uncertainty of ±0.9 per meg associated with the stability of the standard air for the annual average $\delta_{atm}(^{18}O)$ in this study. This uncertainty corresponds to an uncertainty of ±0.13 per meg a^{-1} for the 10-year-long secular trend.

We have examined the influence of the amount fraction of CO_2 in sample air on the $\delta(O_2/N_2)$ measured on a mass spectrometer in past studies (Ishidoya et al., 2003; Ishidoya and Murayama, 2014). In this study, we also experimentally examined the influences of the amount fraction of CO_2 and the $\delta(O_2/N_2)$ on $\delta_{atm}(^{18}O)$. Figure 3a shows typical examples of the relationships between the measured $\delta_{atm}(^{18}O)$ of the air sample and the amount fraction of CO_2. To obtain these relationships, a small amount of pure CO_2 was added to the flow line of the continuous measurement system during the analysis of standard air, or 1-L flasks were analysed before and after a small amount of pure CO_2 was added to the flasks. The precision of the measurements of the

https://doi.org/10.5194/egusphere-2024-654
Preprint. Discussion started: 3 April 2024

flask air samples was about ±4 per meg. As seen in Figure 3a, $\delta_{atm}(^{18}O)$ increased linearly with increasing amount fractions of CO_2. We therefore decided to correct the $\delta_{atm}(^{18}O)$ values by using amount fractions of CO_2 that were measured simultaneously. Figure 3b shows the relationships between the measured $\delta_{atm}(^{18}O)$ values of the air samples and their $\delta(O_2/N_2)$. To obtain these relationships, $\delta_{atm}(^{18}O)$ and $\delta(O_2/N_2)$ were measured for 1-L flasks or 48-L cylinders before and after pure N_2 was added to them. One-litre flasks were filled with the air in the cylinders for the analyses. It is apparent from Figure 3b that we did not find a clearly increasing or decreasing trend of $\delta_{atm}(^{18}O)$, at least when the $\delta(O_2/N_2)$ was decreasing by about –8000 per meg. We therefore decided that we would not correct the $\delta_{atm}(^{18}O)$ values for the changes of the simultaneously measured $\delta(O_2/N_2)$. It is noteworthy that we obtained a different result—an increase of $\delta_{atm}(^{18}O)$ with a decrease of $\delta(O_2/N_2)$—in our earlier experiments in 2013 that involved use of flasks. We have not yet clarified the cause(s), but we expect the results shown in Figure 3b are valid because we repeatedly obtained results that were consistent between flasks and cylinders.

2.2 Box model for simultaneous analysis of $\delta_{atm}(^{18}O)$ and $\delta(O_2/N_2)$

The box model used in this study is the same as that described by Bender et al. (1994). Equation (3) is the mass balance equation for $\delta_{atm}(^{18}O)$.

$$\frac{d\delta_{atm}(^{18}O)}{dt} = (\varepsilon_{MR}r_{MR} + \varepsilon_{PR}r_{PR} + \varepsilon_{DR}r_{DR} - \varepsilon_{LE})R_{Res} + (\delta_{PS} - \delta_{atm})R_{PS}$$
$$+\varepsilon_{OR}R_{OR} + (\delta_{OW} - \delta_{atm})R_{OP} + \varepsilon_{TS}R_{TS} + \varepsilon_{ST}R_{ST}, \quad (3)$$

where r_{MR}, r_{PR}, and r_{DR} are the relative ratios of the Mehler reaction, photorespiration, and dark respiration to the total O_2 consumption associated with terrestrial respiration, and ε_{MR}, ε_{PR}, ε_{DR}, ε_{LE}, and ε_{OR} denote the isotope effects of the Mehler reaction, photorespiration, dark respiration, leaf water enrichment, and marine respiration, respectively. We used values of 15.3, 21.2, 18, 0.7, and 18.9 ‰ for ε_{MR}, ε_{PR}, ε_{DR}, ε_{LE}, and ε_{OR}, respectively, following Bender et al. (1994). ε_{TS} and ε_{ST} denote the isotope effects of air exchange between the troposphere and stratosphere. We assumed the isotopic ratios of the terrestrial and marine O_2 produced via photosynthesis, δ_{PS} and δ_{OW}, to be 4.4 and 0 ‰, respectively, for the steady state. R_{Res}, R_{PS}, R_{OR}, and R_{OP} represent the relative ratios of the annual amounts of O_2 from terrestrial respiration, marine respiration, terrestrial production, and marine production, respectively, to the total amount of O_2 in the atmosphere. R_{TS} and R_{ST} denote the ratios of the annual fluxes of O_2 between the troposphere and stratosphere, respectively. The box model also calculates the amount fraction of atmospheric O_2, $y(O_2)$ by solving the following mass balance equation:

$$\frac{dy(O_2)}{dt} = (r_{MR} + r_{PR} + r_{DR})R_{Res} + R_{PS} + R_{OR} + R_{OP} + R_{TS} + R_{ST} \quad (4)$$

https://doi.org/10.5194/egusphere-2024-654
Preprint. Discussion started: 3 April 2024

Here, y stands for the dry amount fraction of gas, as recommended by the IUPAC Green Book (Cohen et al., 2007). To compare with the observed results for $\delta(O_2/N_2)$, the amount fraction of O_2 calculated by the box model was converted to $\delta(O_2/N_2)$.

All values for the isotope effects and each relative ratio of the respiration processes were the same as those reported by Bender et al. (1994). We assumed the value of terrestrial O_2 production, P_T, to be 16.7 Pmol a^{-1}, which is the value reported by Hoffmann et al. (2004). The marine O_2 production, P_O, was assumed to be half that of P_T. It is known that mass-independent isotopic fractionation of ^{17}O and ^{18}O between O_3 and CO_2 occurs in the stratosphere via photochemical processes (e.g., Gamo et al., 1989; Thiemens, 1999). Bender et al. (1994) have estimated the isotopic effect on atmospheric O_2 by scaling the $\delta(^{18}O)$ of CO_2 and calculated that it would depress $\delta_{atm}(^{18}O)$ by 0.4 ‰, considering the turnover time between the troposphere and the stratosphere. Luz et al. (1999) have shown that the global $\Delta(^{17}O)$ budget supports their result and have estimated the stratospheric isotope effect on $\delta_{atm}(^{18}O)$ to be 0.3 ‰. In this study, the flux between the troposphere and stratosphere was set to 2500 Pmol a^{-1}, which is approximately 100 times the flux from the biosphere (Luz et al., 1999). ε_{ST}, which is the diminution of $\delta(^{18}O)$ due to the O_2 that returns from the stratosphere to the troposphere, is currently considered to be so small that it is impossible to actually detect it in the stratosphere. As a rough estimate, considering that the value of $\Delta(^{17}O)$ is –1.5 per meg (Luz et al., 1999), ε_{ST} is expected to be about –3 per meg. Here, ε_{ST} was set to –4 per meg so that the diminution of $\delta_{atm}(^{18}O)$ at equilibrium was –0.4 ‰. Because there are no isotopic effects during the transport of air from the troposphere to the stratosphere, ε_{TS} should be zero.

The $\delta(^{18}O)$ of stratospheric O_2 has been observed with high precision by balloon experiments and is known to decrease significantly with increasing altitude because of gravitational separation (e.g., Ishidoya et al., 2013b; Sugawara et al., 2018). At an altitude of 35 km over Japan, $\delta(^{18}O)$ is lower than the tropospheric value by approximately –100 per meg, which is anomalously lower than that expected on the basis of photochemical diminution. The implication is that enrichment of approximately 5 per meg is permanently occurring in the troposphere because of gravitational separation in the stratosphere (Ishidoya et al., 2021). It is currently uncertain how gravitational separation affects the process by which isotopically light oxygen is transported to the troposphere through troposphere–stratosphere exchange. This uncertainty complicates the problem of inter-annual $\delta_{atm}(^{18}O)$ change and suggests that gravitational separation may be involved in small fluctuations in the DME.

With these initial settings, we were able to reach a steady state after a 5000-year simulation, and we found that the equilibrium value of $\delta_{atm}(^{18}O)$ was 20.85 ‰. This result is similar to the model result of 20.8 ‰ reported by Bender et al. (1994). Hereafter, the box model results are discussed based on the differences from this equilibrium value. The turnover time of O_2 in the steady state was 1520 years, which is longer than the 1200 years estimated by Bender et al. (1994). In model calculations for the interpretation of long-term changes, we used the steady-state condition described above as the initial condition, and we performed some calculations by adding long-term changes to GPP, photorespiration, and $\delta_{LW}(^{18}O)$ (see details in Sect. 3.3).

https://doi.org/10.5194/egusphere-2024-654
Preprint. Discussion started: 3 April 2024

The box model was suitable for simulations if we assumed that long-term and global changes occurred over timeframes of hundreds to thousands of years. The box model naturally ignores atmospheric transport processes, and it is difficult to define the box atmosphere at local and regional spatial scales. There is hence a theoretical limit to the application of the box model to short-timescale phenomena. However, we tried to use this box model as a first step to understand the diurnal and seasonal changes of $\delta_{atm}(^{18}O)$ recently observed by high-precision measurements. Because $\delta(O_2/N_2)$ was also observed at the same time during this study, the relationships between $\delta_{atm}(^{18}O)$ and $\delta(O_2/N_2)$ provided information about the usefulness of the box model simulations. For the simulations of diurnal changes, the intensities of terrestrial O_2 consumption and production were approximated by a simple function, which became a maximum at noon and zero during the night. Seasonal variations were also simulated by a simple sinusoidal function. We then tuned the magnitude of R_{Res} ($=R_{ps}$) so that the amplitude of the modelled $\delta(O_2/N_2)$ variation was close to the observed results.

2.3 Numerical simulations of $\delta_{LW}(^{18}O)$ using the 3-D model MIROC5-iso

We simulated $\delta_{LW}(^{18}O)$ using a stable water isotope-enabled general circulation model named MIROC5-iso (Okazaki and Yoshimura, 2017, 2019). MIROC5-iso is the fifth generation of the Model for Interdisciplinary Research on Climate (MIROC5; Watanabe et al., 2010). The stable water isotopes were implemented to the atmospheric and land-surface components following Jouzel et al. (1987) and Yoshimura et al. (2006). The MIROC5-iso calculates the isotopic ratio of atmospheric water vapor, precipitation, and reservoirs at ground level, including soil water and leaf water, with the equilibrium and kinetic fractionation at all phase transitions. The $\delta_{LW}(^{18}O)$ is calculated by considering water conveyance driven by transpiration and diffusive isotopic movement (i.e., “back diffusion”). The transpired water drawn up from the root zone layers is calculated by weighting the isotope ratio of soil water by root density. The transpiration fluxes of the water isotopes were calculated by the bulk method with the bulk exchange coefficient of Sellers et al. (1996), and the equilibrium and kinetic fractionations from liquid to gas at the stoma were considered.

In this study, MIROC5-iso was forced by observed sea surface temperature, sea ice concentration, observed greenhouse gases (carbon dioxide, methane, and chlorofluorocarbons), ozone, and changes of land use. The isotopic compositions of sea surface water and sea ice were kept constant and assumed to be 0 ‰ and 3 ‰, respectively, as in Joussaume and Jouzel (1993). The model resolution was set to T42 (approximately 280 km at the equator) with 40 vertical levels. After running MIROC5-iso for 100 years with the condition of AD 1871 for spin-up, we ran the model for AD 1871–2022.

https://doi.org/10.5194/egusphere-2024-654
Preprint. Discussion started: 3 April 2024

3 Results and Discussion

3.1 Diurnal variations of $\delta_{atm}(^{18}O)$ and $\delta(O_2/N_2)$

Figure 4a shows the average diurnal cycles of $\delta_{atm}(^{18}O)$, $\delta(O_2/N_2)$, the amount fraction of CO_2, and $\delta(Ar/N_2)$ for each season observed at TKB during 2013–2022. $\delta(Ar/N_2)$ was defined in the same way as $\delta(O_2/N_2)$ but for the $^{40}Ar/^{14}N^{14}N$ ratio. The error bands shown in Figure 4a indicate year-to-year variations of the average diurnal cycles ($\pm 1\sigma$). In this study, we needed to remove any natural or artificial fractionation of $^{18}O^{16}O$ and $^{16}O^{16}O$, other than the processes associated with the DME from the observed $\delta_{atm}(^{18}O)$. For this purpose, we used the observed diurnal $\delta(Ar/N_2)$ cycle, which is driven by the night-time vertical temperature gradient (Adachi et al., 2006) and artificial inlet fractionation induced by radiative heating of an air intake (e.g., Blaine et al., 2006). The $\delta(Ar/N_2)$ underwent a slight diurnal cycle with a maximum in the early morning (Figure 4a), and the difference between the maximum and minimum was about 4–6 per meg. It is difficult to specify the cause of the diurnal cycle, but it may result from natural variations due to a night-time vertical temperature gradient at the inland TKB site, because Adachi et al. (2006) have reported much larger enrichment of $\delta(Ar/N_2)$ by 100 per meg at the centre of a wide desert during the night. We therefore decided to correct the observed values for thermally diffusive fractionation following the method used by Ishidoya et al. (2014, 2022) and to use the corrected values for our discussion of diurnal variations. Specifically, we subtracted $(1.55/16.2) \times \delta(Ar/N_2)$ from the observed $\delta_{atm}(^{18}O)$. The coefficients 1.55 and 16.2 are the $\delta_{atm}(^{18}O)$ / $\delta(Ar/N_2)$ ratios determined by laboratory experiments (Ishidoya et al., 2013b). In a similar manner, we also corrected the $\delta(O_2/N_2)$ for thermally diffusive fractionation by subtracting $(4.57/16.2) \times \delta(Ar/N_2)$ from the measured $\delta(O_2/N_2)$. The coefficient 4.57/16.2 is the $\delta(O_2/N_2)$ / $\delta(Ar/N_2)$ ratio from the same laboratory experiments. The maximum corrections were 0.3 and 1.0 per meg for $\delta_{atm}(^{18}O)$ and $\delta(O_2/N_2)$, respectively. The correction for the amount fraction of CO_2 was negligibly small.

$\delta_{atm}(^{18}O)$ exhibited a clear diurnal cycle with a daytime minimum, especially in summer (Figure 4a). $\delta_{atm}(^{18}O)$ varied out of phase with $\delta(O_2/N_2)$, and the ratio of the amplitude of the diurnal $\delta_{atm}(^{18}O)$ cycles to those of $\delta(O_2/N_2)$ was substantially larger in summer than in winter. Figure 4a also shows the diurnal cycles of $\delta_{atm}(^{18}O)$ and $\delta(O_2/N_2)$ simulated by the box model described in section 2.2. The simulations were carried out under two conditions, one was the case when we ignored marine respiration and the production of O_2 (R_{OR} and R_{OP}), and the other was the case when we ignored terrestrial respiration and the production of O_2 (R_{Res} and R_{PS}). In both cases, the R_{Res} and R_{PS} (or R_{OR} and R_{OP}) in the model were adjusted to reproduce the observed seasonal $\delta(O_2/N_2)$ cycle subject to the constraint that the daily average $R_{Res} = R_{PS}$ (or $R_{OR} = R_{OP}$). The initial value of the $\delta_{atm}(^{18}O)$ relative to ocean water was then adjusted arbitrarily to establish a steady state for the simulated $\delta_{atm}(^{18}O)$. The $\delta(^{18}O)$ values relative to ocean water in the steady state were 22.0 and 18.9 ‰ for the case when we considered only terrestrial or only marine respiration/production, respectively. We found that the general characteristics of the diurnal cycles of $\delta_{atm}(^{18}O)$

https://doi.org/10.5194/egusphere-2024-654
Preprint. Discussion started: 3 April 2024

and $\delta(O_2/N_2)$ were reproduced by the simulated $\delta_{atm}(^{18}O)$ for both cases when we considered only terrestrial or only marine processes (Figure 4a).

To determine the cause(s) of the observed diurnal $\delta_{atm}(^{18}O)$ cycles, we examined the relationships between the observed $\delta_{atm}(^{18}O)$ and $\delta(O_2/N_2)$ (Figure 4b), and those for $\delta(O_2/N_2)$ and the amount fraction of CO_2 (Figure 4c). The $\delta_{atm}(^{18}O)$ / $\delta(O_2/N_2)$ ratios were −0.017 and –0.006 per meg (per meg)$^{-1}$ in summer and winter, respectively. In Figure 4b, we also plot the relationship between the simulated $\delta_{atm}(^{18}O)$ and $\delta(O_2/N_2)$. We found the simulated ratios to be –0.017 and –0.019 per meg (per meg)$^{-1}$ when we considered only terrestrial or only marine respiration/production, respectively. These ratios were much closer to the ratio observed in summer than in winter. The O_2 and CO_2 exchange ratios (ER, $-\Delta O_2 \Delta CO_2^{-1}$) calculated from the $\delta(O_2/N_2)$ and the amount fraction of CO_2 shown in Figure 4c, were 1.08 and 1.46 in summer and winter, respectively. An oxidative ratio (OR, $-\Delta O_2 \Delta CO_2^{-1}$) of 1.05–1.1 is expected for terrestrial biosphere activities , and ratios of 1.17, 1.44, and 1.95 are expected for combustion of solid fuel, liquid fuel, and natural gas, respectively (Keeling, 1988; Severinghaus, 1995). The ER refers to the exchange between the atmosphere and organisms or ecosystems, whereas the OR reflects the stoichiometry of specific materials, in accord with Faassen et al. (2023) and Ishidoya et al. (2024). The ORs therefore suggested that the diurnal $\delta(O_2/N_2)$ cycle observed in summer could be attributed mainly to terrestrial biosphere activities, whereas that in winter was due to fossil fuel combustion. The observed wintertime ER of 1.46 was also consistent with the average OR of 1.52 ± 0.1 for fossil fuel consumption (hereafter referred to as "OR_{FF}") for the Kanto area, which includes TKB, of about 1.7×10^4 km^2, calculated using the data on fossil fuel consumption reported by the Agency of Natural Resources and Energy (https://www.enecho.meti.go.jp/statistics/energy_consumption/ec002/results.html#headline2, last access: 28 March 2024, in Japanese) (Ishidoya et al., 2020). The implication is therefore that the isotopic discrimination of O_2 during activities of the terrestrial biosphere was the main cause of the observed summertime diurnal $\delta_{atm}(^{18}O)$ and $\delta(O_2/N_2)$ cycles, and the isotopic discrimination of O_2 during fossil fuel combustion was very small or negligible.

The simulated diurnal cycle of $\delta_{atm}(^{18}O)$ and the $\delta_{atm}(^{18}O)$ / $\delta(O_2/N_2)$ ratio for the case when only terrestrial processes were considered were very similar to those for the case when only marine processes were considered. This similarity was due to the small difference between the isotopic discriminations of the terrestrial and marine processes (22.0 – 18.9 = 3.1 ‰). We could therefore estimate the variations of the observed $\delta(O_2/N_2)$ driven by the total activities of the terrestrial and marine biosphere (hereafter referred to as "$\delta_{BIO}(O_2/N_2)$") by dividing the observed variations in $\delta_{atm}(^{18}O)$ by the ratio of the simulated $\delta_{atm}(^{18}O)$ / $\delta(O_2/N_2)$ of about –0.017 to –0.019 per meg (per meg)$^{-1}$. We could then estimate the variations of $\delta(O_2/N_2)$ driven by fossil fuel combustion (hereafter referred to as "$\delta_{FF}(O_2/N_2)$") by subtracting the $\delta_{BIO}(O_2/N_2)$ from the observed $\delta(O_2/N_2)$. This method, hereafter referred to as the "$\delta_{atm}(^{18}O)$-method", enabled us to remove the impact on $\delta(O_2/N_2)$ of not only the activities of the terrestrial biosphere but also the contributions due to the air–sea O_2 flux, which is driven mainly by activities in the marine biosphere (e.g., Nevison et al., 2012; Eddebbar et al., 2017), from the estimated $\delta_{FF}(O_2/N_2)$. Figure 5 shows the $\delta_{BIO}(O_2/N_2)$

https://doi.org/10.5194/egusphere-2024-654
Preprint. Discussion started: 3 April 2024

and $\delta_{FF}(O_2/N_2)$ estimated by the $\delta_{atm}(^{18}O)$-method for each season. The largest amplitudes of the diurnal $\delta_{BIO}(O_2/N_2)$ and $\delta_{FF}(O_2/N_2)$ cycles were in summer and winter, respectively. For comparison, we separated the contributions of terrestrial biosphere activities and fossil fuel combustion to the observed $\delta(O_2/N_2)$ based on the observed ER and amount fraction of CO_2 (hereafter referred to as "ER-method"). For this purpose, (1) we assumed that the diurnal cycle of the amount fraction of CO_2 was driven by terrestrial biosphere activities and fossil fuel combustion, (2) we ignored the contribution of the air–sea O_2 flux on $\delta(O_2/N_2)$, and (3) we assumed the OR for activities in the terrestrial biosphere to be 1.1 and the OR_{FF} to be 1.4, 1.5, 1.6, or 1.7. Figure 5 shows the $\delta(O_2/N_2)$ driven by terrestrial biosphere activities and fossil fuel combustion estimated by the ER-method. The results agreed well with the $\delta_{BIO}(O_2/N_2)$ and $\delta_{FF}(O_2/N_2)$ for all seasons, especially when we chose the OR_{FF} to be 1.6 or 1.7, which are higher and lower than those expected from liquid fuel and natural gas fuel combustion, respectively. The implication is therefore that the diurnal $\delta_{FF}(O_2/N_2)$ cycles at TKB were driven by car traffic (liquid fuels) and household gas consumption. It is noteworthy that propane ($CH_3CH_2CH_3$), for which the OR_{FF} is 1.67 for complete combustion, should also be considered as the household gas consumed in the TKB area.

To determine whether variations of $\delta_{atm}(^{18}O)$ on hourly to daily timeframes were observable, we plotted typical examples in Figure 6 of rolling averages calculated over 300 cycles (5 hours) and 1100 cycles (19 hours) of mass spectrometric measurements of $\delta_{atm}(^{18}O)$ and $\delta(O_2/N_2)$. The summertime graphs (Figure 6a) clearly showed that the $\delta_{atm}(^{18}O)$ varied in antiphase with $\delta(O_2/N_2)$ on timescales of both 5 and 19 hours. The ratios of $\delta_{atm}(^{18}O)$ / $\delta(O_2/N_2)$ were –0.017 per meg (per meg)$^{-1}$ for data averaged over both 5 h and 19 h. This result agreed with that obtained from the summertime average diurnal cycle (vide supra). In contrast, there was no clear correlation between variations of $\delta_{atm}(^{18}O)$ and $\delta(O_2/N_2)$ in winter (Figure 6b). We could distinguish some short-term $\delta_{atm}(^{18}O)$ variations (Figure 6b), but the causes were unclear. The variations may be partly due to activities in the biosphere, because the $\delta_{atm}(^{18}O)$ in winter showed small but substantial diurnal cycles of $\delta_{atm}(^{18}O)$ and $\delta_{BIO}(O_2/N_2)$ (Figure 4a and 5a). These characteristics suggest that we could apply the $\delta_{atm}(^{18}O)$-method to resolve temporal variations of $\delta_{BIO}(O_2/N_2)$ and $\delta_{FF}(O_2/N_2)$ separately on timeframes of several hours to day-to-day. Similar separation has been carried out for CO_2 based on the simultaneous analysis of the $\Delta(^{14}C)$ and amount fraction of CO_2 (e.g., Basu et al., 2020) or based on the simultaneous analysis of $\delta(O_2/N_2)$ and the amount fraction of CO_2 by assuming an average OR_{FF} based on a statistical assessment (Pickers et al., 2022). The $\delta_{atm}(^{18}O)$-method may have some advantages compared with methods used in previous studies because we could apply it without assuming any OR_{FF} with a temporal resolution of 5 hours or perhaps even shorter.

https://doi.org/10.5194/egusphere-2024-654
Preprint. Discussion started: 3 April 2024

3.2 Seasonal cycles of $\delta_{atm}(^{18}O)$ and $\delta(O_2/N_2)$

Figure 7a shows the monthly mean values of $\delta_{atm}(^{18}O)$ and $\delta(O_2/N_2)$ at TKB during 2013–2022. To reduce local effects of fossil fuel combustion around TKB, we extracted the successive maxima of $\delta(O_2/N_2)$ for 4320 cycles (3 days) of mass spectrometric measurements to calculate the monthly mean values of $\delta(O_2/N_2)$ plotted in Figure 7a. In contrast, all data were used to calculate the monthly mean values of $\delta_{atm}(^{18}O)$ to reduce their standard errors, because fossil fuel combustion did not change $\delta_{atm}(^{18}O)$ significantly, as discussed in section 3.1. We removed anomalous $\delta_{atm}(^{18}O)$ data from the plot during four months when the mass spectrometer was producing unreliable results. Figure 7a therefore shows 116 and 120 $\delta_{atm}(^{18}O)$ and $\delta(O_2/N_2)$ data, respectively. Some seasonal and interannual variations are apparent in Figure 7a, not only for $\delta(O_2/N_2)$, which has been reported in many past studies (Keeling and Manning, 2014), but also for $\delta_{atm}(^{18}O)$. We examined the observed average seasonal cycle and secular trend of $\delta_{atm}(^{18}O)$, and in the following paragraphs we discuss the implications thereof for the oxygen, carbon, and water cycles.

Figure 7b shows the average seasonal cycles of $\delta_{atm}(^{18}O)$ and $\delta(O_2/N_2)$ at TKB during 2013–2022. The $\delta(O_2/N_2)$ values in this figure are the values after contributions from the solubility changes in the ocean were removed. For this purpose, we used the seasonal $\delta(Ar/N_2)$ cycle, which is driven mainly by the air–sea heat flux at the surface (e.g., Keeling et al., 2004; Ishidoya et al., 2021; Morgan et al., 2021). Specifically, the average seasonal cycle of $\delta(Ar/N_2)$ at TKB (Ishidoya et al., 2021), multiplied by a coefficient of 0.9 derived from differences in the solubilities of O_2 and Ar (Weiss, 1970), was subtracted from the average seasonal cycle of $\delta(O_2/N_2)$. We applied this correction so that we could discuss the variations of $\delta(O_2/N_2)$ associated with only the DME. The peak-to-peak amplitude of the corrected seasonal $\delta(O_2/N_2)$ cycle was smaller than that of the uncorrected seasonal $\delta(O_2/N_2)$ cycle by about 7 per meg. It is apparent in Figure 7b that the $\delta_{atm}(^{18}O)$ varied seasonally, roughly in antiphase to the seasonal cycle of $\delta(O_2/N_2)$. The minimum of the seasonal $\delta_{atm}(^{18}O)$ cycle appeared in late summer to early autumn, and the peak-to-peak amplitude was about 2 per meg. The maximum of the seasonal $\delta(O_2/N_2)$ cycle occurred in summer, and its peak-to-peak amplitude was 113 per meg.

Keeling (1995) expected $\delta_{atm}(^{18}O)$ to be lower in summer than in winter by 2 per meg based on the assumption that the 100 per meg seasonal increase of $\delta(O_2/N_2)$ was driven by the input of photosynthetic O_2, the $\delta(^{18}O)$ of which is about 20 ‰ lower than $\delta_{atm}(^{18}O)$. Although his estimation was relatively simple, it reproduced the general characteristics of the seasonal $\delta_{atm}(^{18}O)$ and $\delta(O_2/N_2)$ cycles observed in the present study well. In Figure 7b, we also plotted the seasonal cycles of $\delta_{atm}(^{18}O)$ and $\delta(O_2/N_2)$ simulated by our box model. The R_{Res}, R_{PS}, R_{OR}, and R_{OP} values in the model were adjusted to reproduce the observed seasonal $\delta(O_2/N_2)$ cycle by imposing the constraints that the annual average $R_{Res} = -R_{PS}$ and $R_{OR} = -R_{OP}$. We then adjusted the initial value of the $\delta_{atm}(^{18}O)$ in the model arbitrarily to establish a steady state for the simulated $\delta_{atm}(^{18}O)$. We set the R_{Res} / R_{OR}

https://doi.org/10.5194/egusphere-2024-654
Preprint. Discussion started: 3 April 2024

(or R_{PS} / R_{OP}) ratio to be 2 for the simulation in Figure 7b. As discussed in section 3.1, changes of that ratio do not substantially change the simulated results of $\delta_{atm}(^{18}O)$.

We found that the box model could reproduce the observed seasonal $\delta_{atm}(^{18}O)$ cycles, although both the seasonal minimum and maximum of the simulated seasonal $\delta_{atm}(^{18}O)$ cycle appeared slightly earlier (by about 1 month) than in the observed cycle represented by a one-harmonic, best-fit curve. To investigate the possible cause(s) of the phase difference, we carried out additional simulations that incorporated three different seasonally varying $\delta_{LW}(^{18}O)$ values into the box model. Figure 7c shows the simulated results along with the one-harmonic, best-fit curve to the observed data. It is apparent from this figure that the appearance of the seasonal minimum/maximum of $\delta_{atm}(^{18}O)$ depended on the seasonal variations of $\delta_{LW}(^{18}O)$. It is also apparent that the observed seasonal cycle of $\delta_{atm}(^{18}O)$ was well reproduced by the simulation that incorporated the $\delta_{LW}(^{18}O)$ represented by the thick dashed blue line in Figure 7c. Some past studies have reported seasonal variations of $\delta_{LW}(^{18}O)$ (e.g., Welp et al., 2008; Plavcová et al., 2018; Cernusak et al., 2022; Liu et al., 2023). Welp et al. (2008) observed the time series of ecosystem water pools at a soybean canopy in Minnesota, USA, from 30 May to 27 September 2006 and found the most extreme enrichment of bulk $\delta_{LW}(^{18}O)$ to be 20 ‰ above xylem water during the early part of the growing season (Figure 1a in their study). Plavcová et al. (2018) and Liu et al. (2023) have also reported less enrichment of $\delta_{LW}(^{18}O)$ toward the end of the vegetation season by about 10–20 ‰, and Cernusak et al. (2022) have reported a strong negative correlation between the $\delta_{LW}(^{18}O)$ and the relative humidity of air based on a recent global meta-analysis. These characteristics are roughly consistent with the $\delta_{LW}(^{18}O)$ represented by the thick dashed blue line in the present study. That line shows decreases of $\delta_{LW}(^{18}O)$ toward the end of the vegetation season similar in magnitude to decreases reported in past studies. The implication is that seasonal variations of $\delta_{atm}(^{18}O)$ are affected substantially by temporal variations of $\delta_{LW}(^{18}O)$. This result also implies that spatiotemporal variations of $\delta_{LW}(^{18}O)$ can be constrained by an inversion analysis that uses the observed $\delta_{atm}(^{18}O)$ and a three-dimensional atmospheric transport model to incorporate biological and water processes associated with the DME.

3.3 Secular trend in $\delta_{atm}(^{18}O)$

Figure 8 shows temporal changes of the annual average $\delta_{atm}(^{18}O)$ observed at TKB. The error band denotes the ±0.9 per meg of the long-term stability of $\delta_{atm}(^{18}O)$ in our standard air (Figure 2). It is apparent in Figs. 8a and 8b that the $\delta_{atm}(^{18}O)$ underwent a slight secular increase of (0.22 ± 0.14) per meg a^{-1} throughout the observation period. This rate was calculated from the difference between the 2013 and 2022 annual average $\delta_{atm}(^{18}O)$, and the uncertainty around the long-term stability was taken into account. The observed secular increasing trend was quite different from the secular decrease of the DME expected by Seibt et al. (2005), which was on the order of 70 per meg over the last 150 years (–0.5 per meg a^{-1}). They calculated the secular change by assuming anthropogenic changes of the terrestrial oxygen cycle from pre- to post-industrial times: (1) a replacement of 3% of terrestrial respiratory O_2 release by biomass burning, (2) a 5% decrease of global terrestrial GPP, (3) a decrease of

https://doi.org/10.5194/egusphere-2024-654
Preprint. Discussion started: 3 April 2024

345 global photorespiration due to the increase of the amount fraction of atmospheric CO_2 by 100 μmol mol^{-1}, (4) a 10 % decrease of stomatal conductance resulting from CO_2 increases and a partial offset of photorespiratory decreases, and (5) a 5 % decrease of the O_2 flux–weighted ^{18}O enrichment of foliage water due to higher contributions of ^{18}O-depleted northern mid-latitude biomes. The fact that the observation period of 10 years in the present study was much shorter than the 150 years discussed in Seibt et al. (2005) makes it difficult to discuss the significance of the difference between the secular trends in the two studies.
350 It would nevertheless be of interest to see if the observed secular trend could be reproduced using our box model. In that case we could explore the applicability of the precise observations of the $\delta_{atm}(^{18}O)$.

To explore that possibility, we carried out calculations in which we assumed that there were long-term changes of (1) GPP, (2) photorespiration, and (3) $\delta_{LW}(^{18}O)$. Note that we considered long-term changes of only terrestrial fluxes for the GPP and photorespiration. Changes of marine photosynthetic/respiratory O_2 fluxes should be included in more detailed future studies.

355 We first assumed that global GPP increased by 0.45 Pg a^{-1} (C equivalents) from 1871 to 2022, which is the average rate of change during 1992–2020 reported by Bi et al. (2022). This rate of change corresponds to a 31 % increase of GPP over 100 years if the GPP was 120 Pg a^{-1} (C equivalents) in 1992 (Figure 6 in Bi et al., 2022).

Second, we assumed an increase of 120 μmol mol^{-1} in the amount fraction of atmospheric CO_2 during the 150 years from pre-industrial times to the present. This increase caused a decrease of global average photorespiration based on Farquhar et al.
360 (1980):

$$\phi = \left(V_{O\_max}/V_{C\_max}\right) \times (O/C) \times (K_C/K_O) \times 10^{-3} \quad (5)$$

where ϕ is the ratio of photorespiration to carboxylation (or total carbon fixation, the amount of which corresponds to the sum of GPP, photorespiration, and the Mehler reaction), (V_{O_max}/V_{C_max}) is the ratio of the maximum oxygenation velocity to the maximum carboxylation velocity of RuP_2 carboxylase-oxygenase (we used 0.21 for this ratio from equation 16 in Farquhar et
365 al. (1980)). *C* and *O* are the partial pressures of CO_2 and O_2, respectively, in equilibrium with their dissolved amount fractions in the chloroplast stroma. We used the partial pressure of CO_2 in air multiplied by 0.7 and the partial pressure of O_2 in air (209.4 mmol mol^{-1}) for *C* and *O*, respectively, following Bender et al. (1994). (K_C/K_O) is the ratio of the Michaelis-Menten constants for carboxylation and oxygenation, respectively (we adopted 460/330 for this ratio from Table 1 in Farquhar et al. (1980)). We calculated ϕ to be 0.31 and 0.22 for CO_2 amount fractions of 280 and 400 ppm, respectively.

370 We then calculated changes of $\delta_{LW}(^{18}O)$ with MIROC5-iso for the period 1871–2022. We considered the water cycle to be in steady state before 1871, and we assumed the global average $\delta_{LW}(^{18}O)$ in 1871 to be 4.4 ‰ based on a previous study for the DME in steady state (Bender et al., 1994), although Hoffmann et al. (2004) have reported a somewhat higher $\delta_{LW}(^{18}O)$ of 5–6 ‰. It should be noted that the original $\delta_{LW}(^{18}O)$ calculated by MIROC5-iso for 1871 was about –0.7 ‰. We arbitrarily

https://doi.org/10.5194/egusphere-2024-654
Preprint. Discussion started: 3 April 2024

shifted all $\delta_{LW}(^{18}O)$ calculated by MIROC5-iso by 5.1 ‰. Clarifying the cause(s) of the low $\delta_{LW}(^{18}O)$ calculated by MIROC5-iso will be a future task. Figure 8c shows the global average $\delta_{LW}(^{18}O)$; $\delta_{LW}(^{18}O)$ underwent a significant secular increase throughout the period. The increase was especially clear after the 1980s, which is the time when there was an increase of the $\delta(^{18}O)$ of precipitation simulated by MIROC5-iso ($\delta_{precip}(^{18}O)$, not shown). Rozanski et al. (1992) have reported that $\delta_{precip}(^{18}O)$ increases with increasing surface air temperature by 0.6 ‰ K^{-1}, and the global average surface air temperature has increased by about 1 K from 1980 to the present. The increase of surface air temperature therefore caused at least part of the simulated secular increase of $\delta_{LW}(^{18}O)$ since 1980. Previous studies have also reported that a lower (larger) relative humidity near the plant stomata enhances (diminishes) $\delta_{LW}(^{18}O)$ (eq. (2) of Hoffmann et al. (2004)). Also, Byrne and O'Gorman (2018) have reported that the relative humidity over land from 40°S to 40°N has decreased secularly since 1980. It is therefore possible that the decrease of relative humidity also contributed to the simulated secular increase of $\delta_{LW}(^{18}O)$ since 1980.

Figures 8a and 8b show $\delta_{atm}(^{18}O)$ simulated by the box model that incorporated the above-mentioned, long-term changes of GPP, photorespiration, and $\delta_{LW}(^{18}O)$. The secular trends in the observed and the simulated $\delta_{atm}(^{18}O)$ agree well with each other within the uncertainties of the observations. Figure 8a shows the respective contributions of GPP, photorespiration, and $\delta_{LW}(^{18}O)$ to the simulated $\delta_{atm}(^{18}O)$. The simulated $\delta_{atm}(^{18}O)$ increased secularly with increasing GPP and $\delta_{LW}(^{18}O)$. This pattern differed from the results simulated by Seibt et al. (2005), who reported a secular decrease of $\delta_{atm}(^{18}O)$ based on assumed secular decreases of GPP and $\delta_{LW}(^{18}O)$ during the last 150 years. In contrast, both the present study and that of Seibt et al. (2005) found a secular decrease of the simulated $\delta_{atm}(^{18}O)$ with decreasing ratio of photorespiration to carboxylation (ϕ). All three components made non-negligible contributions to the simulated $\delta_{atm}(^{18}O)$. The contributions of ϕ and $\delta_{LW}(^{18}O)$ almost cancelled each other in the simulation of the present study. As a result, the observed secular increase of $\delta_{atm}(^{18}O)$ was driven mainly by the contribution of the secular increase of GPP. In our simulation, GPP increased from 83 to 120 Pg a^{-1} (C equivalents) during 1871–1992 in accord with Bi et al. (2022), and ϕ decreased from 0.31 to 0.22 during that period. If we assume the ratio of the Mehler reaction to carboxylation to have been 0.1 throughout that period, then the calculated photorespiration decreased slightly from 44 and 39 Pg a^{-1} (C equivalents) during 1871–1992, while carboxylation increased from 141 to 176 Pg a^{-1} (C equivalents) during the same period. The implication is that the decrease of photorespiration (5 Pg a^{-1} (C equivalents)) during that period is not enough to explain the increase of GPP by 37 Pg a^{-1} (C equivalents)). A similar increase of global GPP during the 20th century has also been reported by Campbell et al. (2017) based on long-term atmospheric carbonyl sulfide (COS) records derived from ice-core, firn, and ambient air samples.

There have been some efforts to evaluate the mechanisms responsible for the increase of global GPP. Madani et al. (2020) have reported an increase of GPP in northern latitudes caused by a reduction of cold-temperature constraints on plant growth. This scenario suggests that there has been an increase of negative carbon-climate feedback in high latitudes, whereas there has been a suggestion of an emerging positive climate feedback in the tropics, mainly due to an increase of the atmospheric vapor

https://doi.org/10.5194/egusphere-2024-654
Preprint. Discussion started: 3 April 2024

pressure deficit. They have also pointed out that models have been struggling to determine how much additional CO_2 is being taken up by plants as a result of increased amount fractions of atmospheric CO_2. In this context, an analysis based on a secular change in $\delta_{atm}(^{18}O)$, which enables estimation of changes of the ratios of carboxylation to global GPP and photorespiration to global GPP, will facilitate better understanding of global CO_2 fertilization processes.

We used the global average secular change of $\delta_{LW}(^{18}O)$ simulated by the MIROC5-iso in this analysis, and we found that it made a substantial contribution to the simulated $\delta_{atm}(^{18}O)$. The implication is that the secular change of the water cycle must be accurate before the observed and simulated secular trends of $\delta_{atm}(^{18}O)$ can be equated. In other words, $\delta_{atm}(^{18}O)$ is a unique tracer for a comprehensive evaluation of global changes of the oxygen, carbon, and water cycles. For example, if the secular increase of the global average amount fraction of atmospheric CO_2 stops without changes of the secular increasing trends of GPP, then the global average $\delta_{atm}(^{18}O)$ will increase faster than the rate shown in Figure 8a. A secular decrease of the global average $\delta_{atm}(^{18}O)$ may also be expected under pessimistic scenarios, such as substantial deforestation (secular decrease of GPP) and an increase of the average global amount fraction of atmospheric CO_2. In both cases, the results are regulated by climate changes such as changes of surface air temperature and aridification that lead to secular changes of $\delta_{LW}(^{18}O)$.

We recognize that secular changes of stratospheric gravitational separation may cause slight secular changes of the surface $\delta_{atm}(^{18}O)$. Ishidoya et al. (2021) have estimated this effect for atmospheric $\delta(Ar/N_2)$ at the surface to be –0.13 and 0.15 per meg a^{-1} when accompanied by a weakening or enhancement of the Brewer–Dobson circulation, respectively. These values correspond to –0.02 and 0.03 per meg a^{-1}, respectively, for $\delta_{atm}(^{18}O)$ if mass-dependent gravitational separation is assumed. The secular trend of $\delta_{atm}(^{18}O)$ due to changes of stratospheric gravitational separation is negligible at present because the changes are much smaller than the uncertainty of the secular trend of the observed $\delta_{atm}(^{18}O)$ at TKB ((0.22 ± 0.14) per meg a^{-1}). If the observation period increases, the uncertainty of the secular trend will be smaller. Consideration of stratospheric gravitational separation changes may therefore be needed in future.

4 Conclusions

We have carried out high-precision measurements of $\delta_{atm}(^{18}O)$ at TKB site since 2013. Clear variations of $\delta_{atm}(^{18}O)$ with a daytime minimum were found for the average diurnal cycles throughout the observation period. The much larger amplitudes of the diurnal $\delta_{atm}(^{18}O)$ cycles in summer than in winter suggest a substantial contribution of the activities in the terrestrial biosphere to the diurnal cycle. The amplitudes and phases of the diurnal $\delta_{atm}(^{18}O)$ and $\delta(O_2/N_2)$ cycles simulated by a box model, which incorporated the terrestrial oxygen cycle, were roughly consistent with the observed diurnal cycles in summer. Seasonal changes of the ERs, calculated from the average diurnal cycles of the $\delta(O_2/N_2)$ and amount fractions of CO_2, also indicated a larger contribution of the activities in the terrestrial biosphere in summer than in winter. We found that the 5h- and

https://doi.org/10.5194/egusphere-2024-654
Preprint. Discussion started: 3 April 2024

19h-averaged $\delta_{atm}(^{18}O)$ also varied in antiphase with $\delta(O_2/N_2)$ in summer. We found that the diurnal cycles of $\delta_{BIO}(O_2/N_2)$ and $\delta_{FF}(O_2/N_2)$, estimated by the $\delta_{atm}(^{18}O)$-method, agreed well with the diurnal $\delta(O_2/N_2)$ cycles driven by activities in the terrestrial biosphere and fossil fuel combustion estimated by the ER-method.

The $\delta_{atm}(^{18}O)$ varied seasonally in antiphase with $\delta(O_2/N_2)$ and was a minimum in the summer. We found the peak-to-peak amplitude of the average seasonal $\delta_{atm}(^{18}O)$ cycle to be about 2 per meg. These characteristics were generally reproduced by the box model, and the seasonal $\delta_{atm}(^{18}O)$ cycle was driven mainly by an input of photosynthetic O_2, the $\delta(^{18}O)$ of which was about 20 ‰ lower than $\delta_{atm}(^{18}O)$. The box model also suggested that the seasonal cycle of $\delta_{atm}(^{18}O)$ was substantially affected by seasonally varying $\delta_{LW}(^{18}O)$, which indicated the usefulness of $\delta_{atm}(^{18}O)$ observations to constrain spatiotemporal variations of $\delta_{LW}(^{18}O)$. There was a secular increase of the $\delta_{atm}(^{18}O)$ by (0.22 ± 0.14) per meg a^{-1} throughout the observation period. To interpret the secular trend, we used the box model to carry out a simulation in which we considered the long-term changes of GPP, photorespiration, and $\delta_{LW}(^{18}O)$. For the calculation of $\delta_{LW}(^{18}O)$, we also used the 3D model MIROC5-iso. We found that all three components made substantial contributions to the simulated $\delta_{atm}(^{18}O)$. In the box model simulation, the contributions of photorespiration and $\delta_{LW}(^{18}O)$ almost cancelled each other. The result was an observed secular increase of $\delta_{atm}(^{18}O)$ driven mainly by the secular increase of GPP. The results imply that the secular decrease of photorespiration was not enough to explain the secular increase of GPP if the ratio of the Mehler reaction to carboxylation did not change throughout the simulation.

In conclusion, we confirmed that precise observations of the spatiotemporal variations of $\delta_{atm}(^{18}O)$ will enable better understanding of the global cycles of O_2, CO_2, and water. However, no relevant observational results have previously been reported. Additional steps should therefore include observations of the $\delta_{atm}(^{18}O)$ at some surface stations in both hemispheres using continuous measurement systems that are similar to the system used in the present study and a newly developed, precise measurement system for flask samples. Two- and three-dimensional models to calculate $\delta_{atm}(^{18}O)$ should be developed to interpret the latitudinal differences of the observed $\delta_{atm}(^{18}O)$ variations. There is also need for improvement of the three-dimensional model simulation of $\delta_{LW}(^{18}O)$, because the original $\delta_{LW}(^{18}O)$ calculated with MIROC5-iso was systematically lower than those reported by past studies. Such progress will better enable detection of the signal of climate changes associated with the DME.

Data availability

The observational data for diurnal cycles and monthly mean values shown in Fig. 4, 6, and 7 are included as electronic supplement to the manuscript. We will deposit the data in an appropriate data archive before the manuscript is accepted for publication.

https://doi.org/10.5194/egusphere-2024-654
Preprint. Discussion started: 3 April 2024

Author contributions

SI designed the study, conducted measurements of $\delta_{atm}(^{18}O)$, $\delta(O_2/N_2)$ and CO_2 amount fractions, and drafted the manuscript. SS conducted the box model simulations. AO conducted the MIROC5-iso simulations. All authors approved the final manuscript.

Competing interests

The authors declare that they have no conflict of interest.

Acknowledgements

This study was partly supported by Japan Society for the Promotion of Science KAKENHI grants (grant nos. 22H05006, 23H00513, and 22H04938) and the Global Environment Research Coordination System from the Ministry of the Environment, Japan (grant no. METI1953).

References

Adachi Y, Kawamura K, Armi L, Keeling R. F.: Diffusive separation of the lower atmosphere. Science, 311, 1429, 2006.

Aoki, N., Ishidoya, S., Matsumoto, N., Watanabe, T., Shimosaka, T., and Murayama, S.: Preparation of primary standard mixtures for atmospheric oxygen measurements with less than 1 μmol mol^{-1} uncertainty for oxygen molar fractions, Atmos. Meas. Tech., 12, 2631–2646, https://doi.org/10.5194/amt-12-2631-2019, 2019.

Barkan, E., and Luz, B.: High precision measurements of $^{17}O/^{16}O$ and $^{18}O/^{16}O$ ratios in H_2O, Rapid Commun. Mass Spectrom.,19, 3737–3742, 2005.

Basu, S., Lehman, S. J., Miller, J. B., Andrews, A. E., Sweeney, C., Gurney, K. R., Xu, X., Southon, J., and Tans, P. P.: Estimating US fossil fuel CO_2 emissions from measurements of ^{14}C in atmospheric CO_2, Proc. Natl. Acad. Sci. U.S.A. 117, 13300–13307, 2020.

Battle, M. O., William Munger, J., Conley, M., Sofen, E., Perry, R., Hart, R., Davis, Z., Scheckman, J., Woogerd, J., Graeter, K., Seekins, S., David, S., and Carpenter, J.: Atmospheric measurements of the terrestrial O_2 : CO_2 exchange ratio of a midlatitude forest, Atmospheric Chemistry and Physics, 19, 8687–8701, https://doi.org/10.5194/acp-19-8687-2019, 2019.

Bender, M., Sowers, T., and Labeyrie, L.: The Dole effect and its variations during the last 130,000 years as measured in the Vostok ice core, Global Biogeochem. Cycles, 8(3), 363–376, 1994.

Bi, W., He, W., Zhou, Y., Weimin, J., Liu, Y., Liu, Y., Zhang, X., Wei, X., and Cheng, N.: A global 0.05° dataset for gross primary production of sunlit and shaded vegetation canopies from 1992 to 2020, Sci. Data 9, 213. https://doi.org/10.1038/s41597-022-01309-2., 2022.

https://doi.org/10.5194/egusphere-2024-654
Preprint. Discussion started: 3 April 2024

Blaine, T. W., Keeling, R. F. and Paplawsky, W. J.: An improved inlet for precisely measuring the atmospheric Ar/N_2 ratio, Atmos. Chem. Phys. 6, 1181-1184, 2006.

Byrne, M.P., and O'Gorman, P.A.: Trends in continental temperature and humidity directly linked to ocean warming, Proc. Natl. Acad. Sci. U.S.A. 115, 4863–4868, 2018.

Campbell, J.E., Berry, J.A., Seibt, U., Smith, S.J., Montzka, S.A., Launois, T. Belviso, S. Bopp, L., and Laine, M.: Large historical growth in global terrestrial gross primary production, Nature, 544(7648), 84-87. doi: 10.1038/nature22030, 2017.

Cernusak, L. A., Barbeta, A., Bush, R., Eichstaedt R., Ferrio, J., Flanagan, L., Gessler, A., Martín-Gómez, P., Hirl, R., Kahmen, A., Keitel., C., Lai, C., Munksgaard, N., Nelson, D., Ogée J., Roden, J., Schnyder, H., Voelker, S., Wang L., Stuart-Williams, H., Wingate, L., Yu, W., Zhao, L., and Cuntz, M.: Do ^{2}H and ^{18}O in leaf water reflect environmental drivers differently?, New Phytol., 235, 41–51, https://doi.org/10.1111/nph.18113, 2022.

Cohen, E. R., Cvitas, T., Frey, J. G., Holmstrom, B., Kuchitsu, K., Marquardt, R., Mills, I., Pavese, F., Quack, M., Stohner, J., Strauss, H., Takami, M., and Thor, A. J.: IUPAC Green Book: 3rd edn., RSC Publishing, ISBN 0854044337, ISBN-13 9780854044337, 2007.

Craig, H.: Standard for reporting concentrations of deuterium and oxygen-18 in natural water, Science, 133, 1833–1834, 1961.

Dole, M.: The relative atomic weight of oxygen in water and in air, J. Am. Chem. Soc., 57, 2731, 1935.

Eddebbar, Y. A., Long, M. C., Resplandy, L., Rödenbeck, C., Rodgers, K. B., Manizza, M., and Keeling, R. F.: Impacts of ENSO on air-sea oxygen exchange: Observations and mechanisms, Global Biogeochem. Cy., 31, 901–921, https://doi.org/10.1002/2017GB005630, 2017.

Faassen, K. A. P., Nguyen, L. N. T., Broekema, E. R., Kers, B. A. M., Mammarella, I., Vesala, T., Pickers, P. A., Manning, A. C., Vilà-Guerau de Arellano, J., Meijer, H. A. J., Peters, W., and Luijkx, I. T.: Diurnal variability of atmospheric O_2, CO_2, and their exchange ratio above a boreal forest in southern Finland, Atmos. Chem. Phys., 23, 851–876, https://doi.org/10.5194/acp-23-851-2023, 2023.

Farquhar, G. D., von Caemmerer, S., and Berry, J. A.: A biochemical model of photosynthetic CO_2 assimilation in leaves of C3 species, Planta, 149, 78–90, 1980.

Gamo, T., Tsutsumi, M., Sakai, H., Nakazawa, T., Tanaka, M., Honda, H., Kubo, H., and Itoh, T., Carbon and oxygen isotopic ratios of carbon dioxide of a stratospheric profile over Japan, Tellus, Ser. B, 41, 127–133, doi:10.1111/j.1600-0889.1989.tb00130.x, 1989.

Hoffmann, G., Suntz, M., Weber, C., Ciais, P., Friedlingstein, P., Heimann, M., Jouzel, J., Kaduk, J., Maier-Reimer, E., Seibt, U., and Six, K.: A model of the Earth's Dole effect, Global Biogeochem. Cycles, 18, GB1008, doi:10.1029/2003GB002059, 2004.

Ishidoya, S., Aoki, S. and Nakazawa, T.: High precision measurements of the atmospheric O_2/N_2 ratio on a mass spectrometer. J. Meteorol. Soc. Jpn. 81, 127–140, 2003.

https://doi.org/10.5194/egusphere-2024-654
Preprint. Discussion started: 3 April 2024

Ishidoya, S., Murayama, S., Takamura, C., Kondo, H., Saigusa, N., Goto, D., Morimoto, S., Aoki, N., Aoki, S., and Nakazawa, T.: O_2:CO_2 exchange ratios observed in a cool temperate deciduous forest ecosystem of central Japan, Tellus B, 65, doi:10.3402/tellusb.v65i0.21120, 2013a.

Ishidoya, S., Sugawara, S., Morimoto, S., Aoki, S., Nakazawa, T., Honda, H., and Murayama, S.: Gravitational separation in the stratosphere – a new indicator of atmospheric circulation, Atmos. Chem. Phys., 13, 8787-8796, doi:10.5194/acp-13-8787-2013, 2013b.

Ishidoya, S., and Murayama, S.: Development of high precision continuous measuring system of the atmospheric O_2/N_2 and Ar/N_2 ratios and its application to the observation in Tsukuba, Japan, Tellus B, 66, 22574, http://dx.doi.org/10.3402/tellusb.v66.22574, 2014.

Ishidoya, S., Tsuboi, K., Matsueda, H., Murayama, S., Taguchi, S., Sawa, Y., Niwa, Y., Saito, K., Tsuji, K., Nishi, H., Y. Baba, Y., Takatsuji, S., Dehara, K., and Fujiwara, H.: New atmospheric O_2/N_2 ratio measurements over the western North Pacific using a cargo aircraft C-130H, SOLA, 10, 23–28, https://doi.org/10.2151/sola.2014-006, 2014.

Ishidoya, S., Sugawara, H., Terao, Y., Kaneyasu, N., Aoki, N., Tsuboi, K., and Kondo, H.: O_2 : CO_2 exchange ratio for net turbulent flux observed in an urban area of Tokyo, Japan, and its application to an evaluation of anthropogenic CO_2 emissions, Atmos. Chem. Phys., 20, 5293–5308, https://doi.org/10.5194/acp-20-5293-2020, 2020.

Ishidoya, S., Sugawara, S., Tohjima, Y., Goto, D., Ishijima, K., Niwa, Y., Aoki, N., and Murayama, S.: Secular change in atmospheric Ar/N_2 and its implications for ocean heat uptake and Brewer–Dobson circulation, Atmos. Chem. Phys., 21, 1357–1373, https://doi.org/10.5194/acp-21-1357-2021, 2021.

Ishidoya, S., Tsuboi, K., Niwa, Y., Matsueda, H., Murayama, S., Ishijima, K., and Saito, K.: Spatiotemporal variations of the $\delta(O_2/N_2)$, CO_2 and δ(APO) in the troposphere over the western North Pacific, Atmos. Chem. Phys., 22, 6953–6970, https://doi.org/10.5194/acp-22-6953-2022, 2022.

Ishidoya, S., Tsuboi, K., Kondo, H., Ishijima, K., Aoki, N., Matsueda, H., and Saito, K.: Measurement report: Method for evaluating CO_2 emissions from a cement plant using atmospheric $\delta(O_2/N_2)$ and CO_2 measurements and its implication for future detection of CO_2 capture signals, Atmos. Chem. Phys., 24, 1059–1077, https://doi.org/10.5194/acp-24-1059-2024., 2024.

Joussaume, S., and Jouzel, J.: Paleoclimatic tracers: An investigation using an atmospheric general circulation model under ice age conditions 2. Water isotopes. J. Geophys. Res., 98(D2), 2807–2830, 1993.

Jouzel, J., Russell, G. L., Suozzo, R. J., Koster, R. D., White, J. W. C., and Broecker, W. S.: Simulations of the HDO and $H_2{}^{18}O$ atmospheric cycles using the NASA GISS general circulation model: The seasonal cycle for present-day conditions. J. Geophys. Res., 92(D12), 14,739–14,760, 1987.

Keeling, R. F.: Development of an interferometric oxygen analyzer for precise measurement of the atmospheric O_2 mole fraction, Ph.D. thesis, Harvard University, Cambridge, 1988.

Keeling, R. F.: The atmospheric oxygen cycle: The oxygen isotopes of atmospheric CO_2 and O_2 and the N_2/O_2 ratio, Rev. Geophys., 1253– 1262, 1995.

https://doi.org/10.5194/egusphere-2024-654
Preprint. Discussion started: 3 April 2024

Keeling, R. F., Blaine, T., Paplawsky, B., Katz, L., At- wood, C., and Brockwell, T.: Measurement of changes in atmospheric Ar/N_2 ratio using a rapid-switching, single-capillary mass spectrometer system, Tellus B, 56, 322–338, https://doi.org/10.3402/tellusb.v56i4.16453, 2004.

Keeling, R. and Manning, A.: Studies of Recent Changes in Atmospheric O_2 Content, in: Treatise on Geochemistry, 2nd edn., Elsevier Inc., 5, 385–404, https://doi.org/10.1016/B978-0-08- 095975-7.00420-4, 2014.

Liu, J., Jiang, C., Wu, H., Guo, L., Zhang, H., and Zhao, Y.: Controls on leaf water hydrogen and oxygen isotopes: a local investigation across seasons and altitude , Hydrol. Earth Syst. Sci., 27, 599–612, https://doi.org/10.5194/hess-27-599-2023, 2023.

Luz, B., Barkan, E., Bender, M. L., Thiemens, M. H., and Boering, K. A.: Triple-isotope composition of atmospheric oxygen as a tracer of biosphere productivity, Nature, 400, 547–550, doi:10.1038/22987, 1999.

Madani, N., Parazoo, N. C., Kimball, J. S., Ballantyne, A. P., Reichle, R. H., Maneta, M., Saatchi, S., Palmer P. I., Liu, Z., and Tagesson, T.: Recent amplified global gross primary productivity due to temperature increase is offset by reduced productivity due to water constraints, AGU Advances, 2, e2020AV000180, https://doi.org/10.1029/2020AV000180, 2020.

Morita, N.: The increased density of air oxygen relative to water oxygen, J. Chem. Soc. Japan, 56, 1291, 1935.

Morgan, E. J., Manizza, M., Keeling, R. F., Resplandy, L., Mikaloff-Fletcher, S. E., Nevison, C. D., Jin, Y., Bent, J. D., Aumont, O., Doney, S. C., Dunne, J. P., John, J., Lima, I. D., Long, M. C., and Rodgers, K. B.: An atmospheric constraint on the seasonal air-sea exchange of oxygen and heat in the extratropics. J. Geophys. Res. Oceans, 126, e2021JC017510. https://doi.org/10.1029/2021JC017510, 2021.

Nevison, C. D., Keeling, R. F., Kahru, M., Manizza, M., Mitchell, B. G., and Cassar N.: Estimating net community production in the Southern ocean based on atmospheric potential oxygen and satellite ocean color data, Glob. Biogeochem. Cycles., 26, GB1020, https://doi.org/10.1029/2011GB004040, 2012.

Okazaki, A., Yoshimura, K.: Development and evaluation of a system of proxy data assimilation for paleoclimate reconstruction, Clim. Past, 13, 379–393, https://doi.org/10.5194/cp-13-379-2017, 2017.

Okazaki, A., Yoshimura, K.: Global evaluation of proxy system models for stable water isotopes with realistic atmospheric forcing, J. Geophys. Res. Atmospheres, 124, 8972–8993. https://doi.org/ 10.1029/2018JD029463, 2019.

Pickers, P. A., Manning, A. C., Le Quéré, C., Forster, G. L., Luijkx, I. T., Gerbig, C., Fleming, L. S., Sturges, W. T.: Novel quantification of regional fossil fuel CO_2 reductions during COVID-19 lockdowns using atmospheric oxygen measurements, Science Advances, 8(16), eabl9250, 2022.

Plavcová, L., Hronková, M., Šimková, M., Květoň , J., Vráblová, M., Kubásek, J., Šantrůček, J.: Seasonal variation of $\delta^{18}O$ and δ^2H in leaf water of Fagus sylvatica L. and related water compartments, J. Plant Physiol., 227, 56–65, 2018.

Rozanski, K., Araguás-Araguás, L., Gonfiantini, R.: Relation between long-term trends of oxygen-18 isotope composition of precipitation and climate, Science, 258(5084):981-985, doi: 10.1126/science.258.5084.981, 1992.

https://doi.org/10.5194/egusphere-2024-654
Preprint. Discussion started: 3 April 2024

Seibt, U., Berry, J.A., Battle, M., Severinghaus, J.P.: Exploring potential anthropogenic changes in the Dole-Morita effect, abstract of the 7th International CO_2 Conference, https://gml.noaa.gov/icdc7/proceedings/abstracts/seibtFF351.pdf, 2005.

Sellers, P., Randall, D.A., Collatz, G.J., Berry, J.A., Field, C.B., Dazlich, D.A., Zhang, C., Collelo, G.D., and Bounoua, L.: A Revised Land Surface Parameterization (SiB2) for Atmospheric GCMS. Part I: Model Formulation. J. Climate, 9, 676–705, 1996.

Severinghaus, J.P., Beaudette, R., Headly, M.A., Taylor, K., Brook, E.J.: Oxygen-18 of O_2 records the impact of abrupt climate change on the terrestrial biosphere, Science, 324, 1432-1434. DOI: 10.1126/Science.1169473., 2009.

Severinghaus, J.: Studies of the terrestrial O_2 and carbon cycles in sand dune gases and in biosphere 2, Ph. D. thesis, Columbia University, New York, 1995.

Sturm, P., Leuenberger, M., Valentino, F. L., Lehmann, B. and Ihly, B.: Measurements of CO_2, its isotopes, O_2/N_2, and 222Rn at Bern, Switzerland, Atmos. Chem. Phys.6, 1991-2004, 2006.

Sugawara, S., Ishidoya, S., Aoki, S., Morimoto, S., Nakazawa, T., Toyoda, S., Inai, Y., Hasebe, F., Ikeda, C., Honda, H., Goto, D., and Putri, F. A., 2018: Age and gravitational separation of the stratospheric air over Indonesia, Atmos. Chem. Phys., 18, 1819-1833, https://doi.org/10.5194/acp-18-1819-2018, 2018.

Thiemens, M. H.: Mass-independent isotope effects in planetary atmospheres and the early solar system, Science, 283, 341–345, doi:10.1126/science.283.5400.341, 1999.

Watanabe, M., Suzuki, T., O'ishi, R., Komura, Y., Watanabe, S., Emori, S., Takemura, T., Chikira, M., Ogura, T., Sekiguchi, M., Takata, K., Yamazaki, D., Yokohata, T., Nozawa, T., Hasumi, H., Tatebe, H., and Kimoto, M.: Improve climate simulated by MIROC5: Mean states, variability, and climate sensitivity, J. Clim., 23(23), 6312–6335, 2010.

Weiss, R. F.: The solubility of nitrogen, oxygen and argon in water and seawater, Deep-Sea Res., 17, 721–735, 1970.

Welp, L. R., Lee, X., Kim, K., Griffis, T.J., Billmark, K.A., and Baker, J.M.: $\delta^{18}O$ of water vapour, evapotranspiration and the sites of leaf water evaporation in a soybean canopy. Plant. Cell Environ., 31, 1214– 1228, 2008.

Yoshimura, K., Miyazaki, S., Kanae, S., and Oki, T.: Iso-MATSIRO, a land surface model that incorporates stable water isotopes, Glob. Planet. Change, 51(1-2), 90–107, 2006.

https://doi.org/10.5194/egusphere-2024-654
Preprint. Discussion started: 3 April 2024

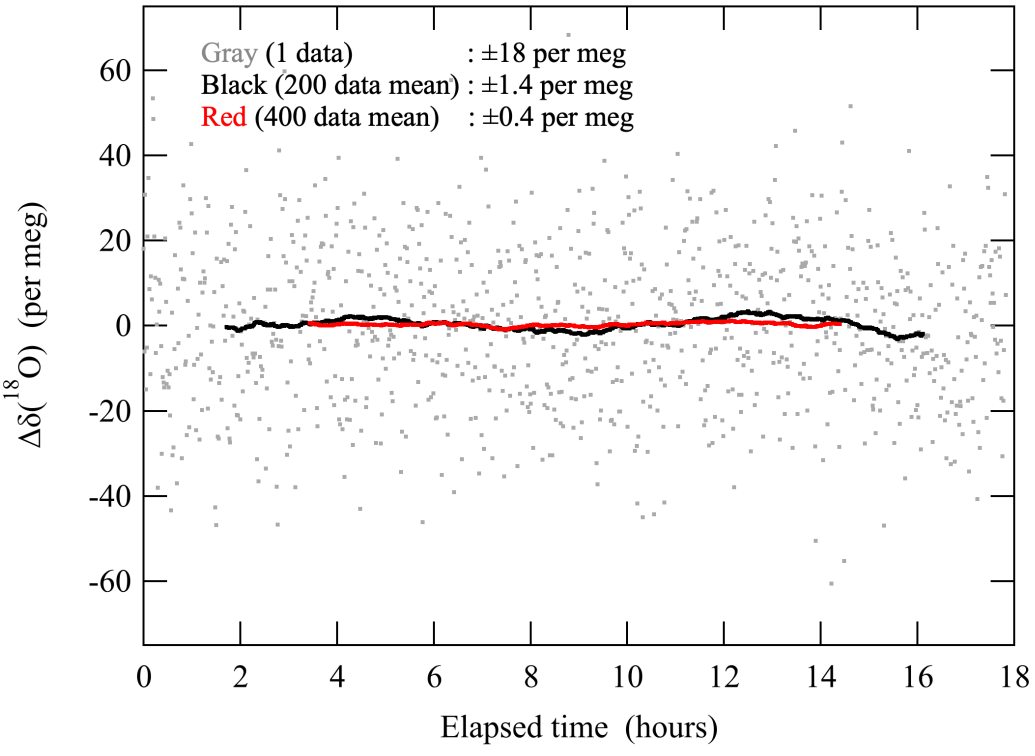

Figure 1: Typical analytical results of the difference (Δ) of the $\delta(^{18}O)$ of standard air against a reference air. Data are shown as deviations from the average value throughout the analysis. Gray dots, black lines, and red lines denote raw data, and averages of 200 and 400 data (corresponding to about 62 seconds, 3.5 hours, and 7 hours), respectively.

https://doi.org/10.5194/egusphere-2024-654
Preprint. Discussion started: 3 April 2024

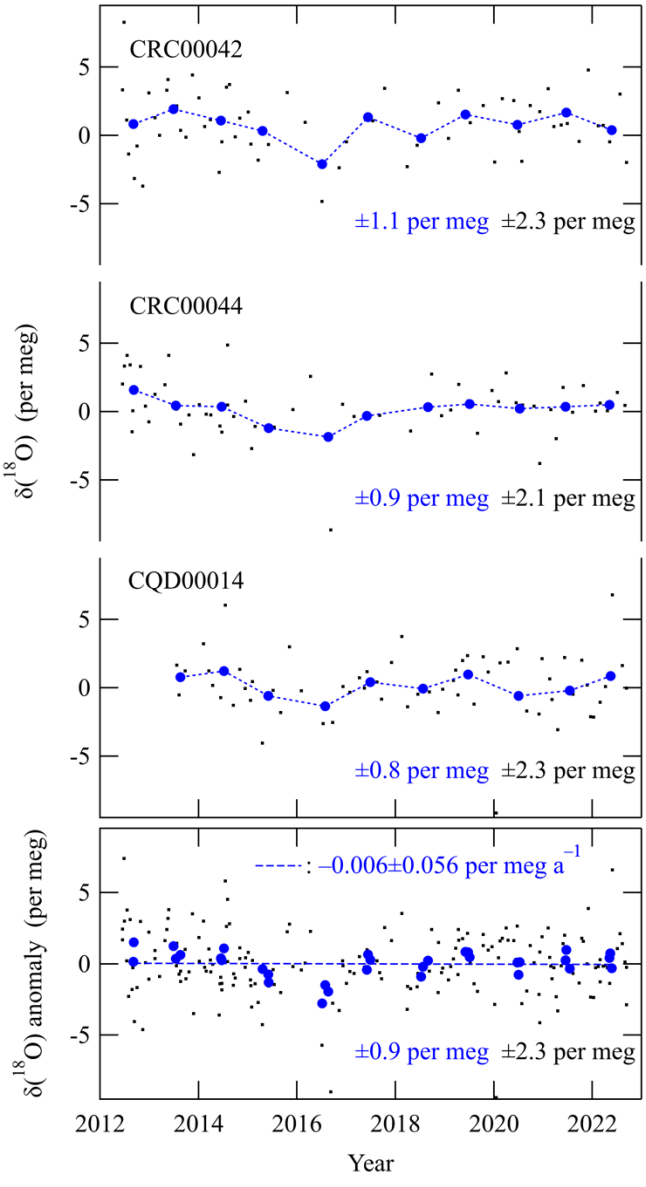

630

Figure 2: (top) Each value (black dots) and the corresponding annual average (blue circles) of $\delta(^{18}O)$ of three secondary standards against the primary standard air. (bottom) Anomalies of $\delta(^{18}O)$ of the three secondary standards. Blue dashed line denotes the regression line fit to the data.

635

https://doi.org/10.5194/egusphere-2024-654
Preprint. Discussion started: 3 April 2024

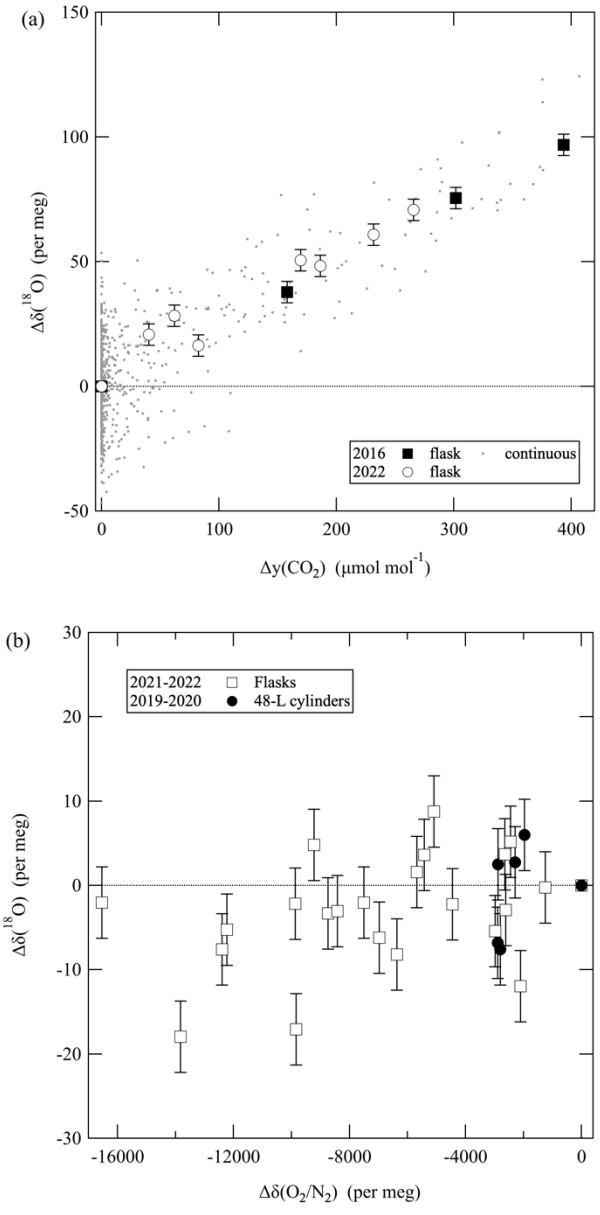

Figure 3: (a) Changes (Δ) of the measured $\delta(^{18}O)$ of air samples as a function of the amount fraction of CO_2. $\Delta y(CO_2)$ represents the difference between the amount fraction of CO_2 of the air sample after and before adding pure CO_2. y stands for the dry amount fraction of gas. (b) Changes of the measured $\delta(^{18}O)$ of the air sample as a function of its $\delta(O_2/N_2)$. $\Delta\delta(O_2/N_2)$ represents the difference

https://doi.org/10.5194/egusphere-2024-654
Preprint. Discussion started: 3 April 2024

between the $\delta(O_2/N_2)$ of the air sample after and before adding pure N_2. Error bars in (a) and (b) indicate uncertainties ($\pm 1\sigma$) for the measurements of air samples in flasks.

645

https://doi.org/10.5194/egusphere-2024-654
Preprint. Discussion started: 3 April 2024

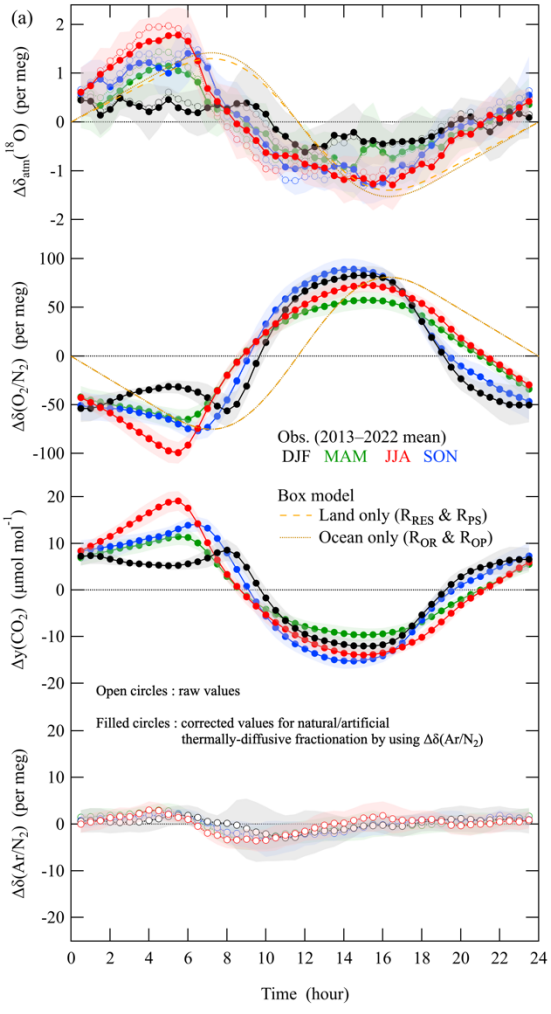

650

https://doi.org/10.5194/egusphere-2024-654
Preprint. Discussion started: 3 April 2024

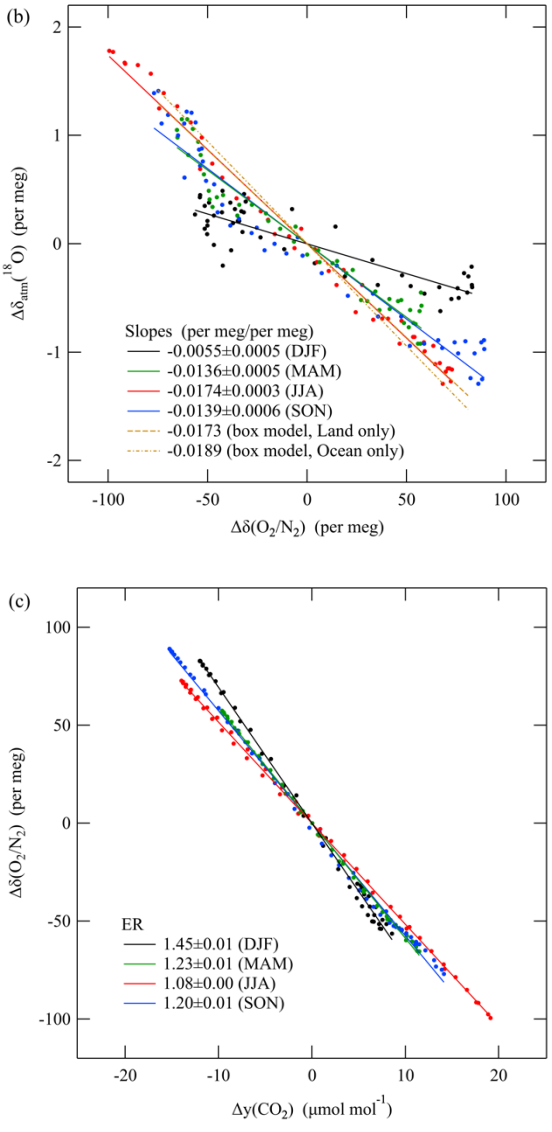

Figure 4: (a) Plots of average diurnal cycles of $\Delta\delta_{atm}(^{18}O)$, $\Delta\delta(O_2/N_2)$, $\Delta y(CO_2)$, and $\Delta\delta(Ar/N_2)$ (open circles) observed at the TKB site during 2013–2022 for each season: December to February (black), March to May (green), June to August (red), and September to November (blue). Error bands indicate year-to-year variations during the observation periods ($\pm1\sigma$). Those of $\Delta\delta_{atm}(^{18}O)$, $\Delta\delta(O_2/N_2)$, and $\Delta y(CO_2)$, corrected for thermally diffusive fractionation, are also plotted (filled circles) (see text). The range of the vertical axis for $\Delta\delta(Ar/N_2)$ was adjusted arbitrarily to facilitate visual assessment of the variations of the observed $\Delta\delta_{atm}(^{18}O)$ due to thermally diffusive fractionation. Average diurnal cycles of $\Delta\delta_{atm}(^{18}O)$ and $\Delta\delta(O_2/N_2)$ that were simulated with a box model are also shown. The simulated values that considered only terrestrial and marine respiration/production are shown by solid and dashed ocher lines, respectively (see text). Δ denotes deviations from the diurnal mean values. (b) Relationships between $\Delta\delta_{atm}(^{18}O)$ and

https://doi.org/10.5194/egusphere-2024-654
Preprint. Discussion started: 3 April 2024

$\Delta\delta(O_2/N_2)$ for the data corrected for thermally diffusive fractionation in (a). Regression lines fitted to the observed and simulated data are also shown. (c) Same as in (b) but for the relationship between $\Delta\delta(O_2/N_2)$ and $\Delta y(CO_2)$.

https://doi.org/10.5194/egusphere-2024-654
Preprint. Discussion started: 3 April 2024

665

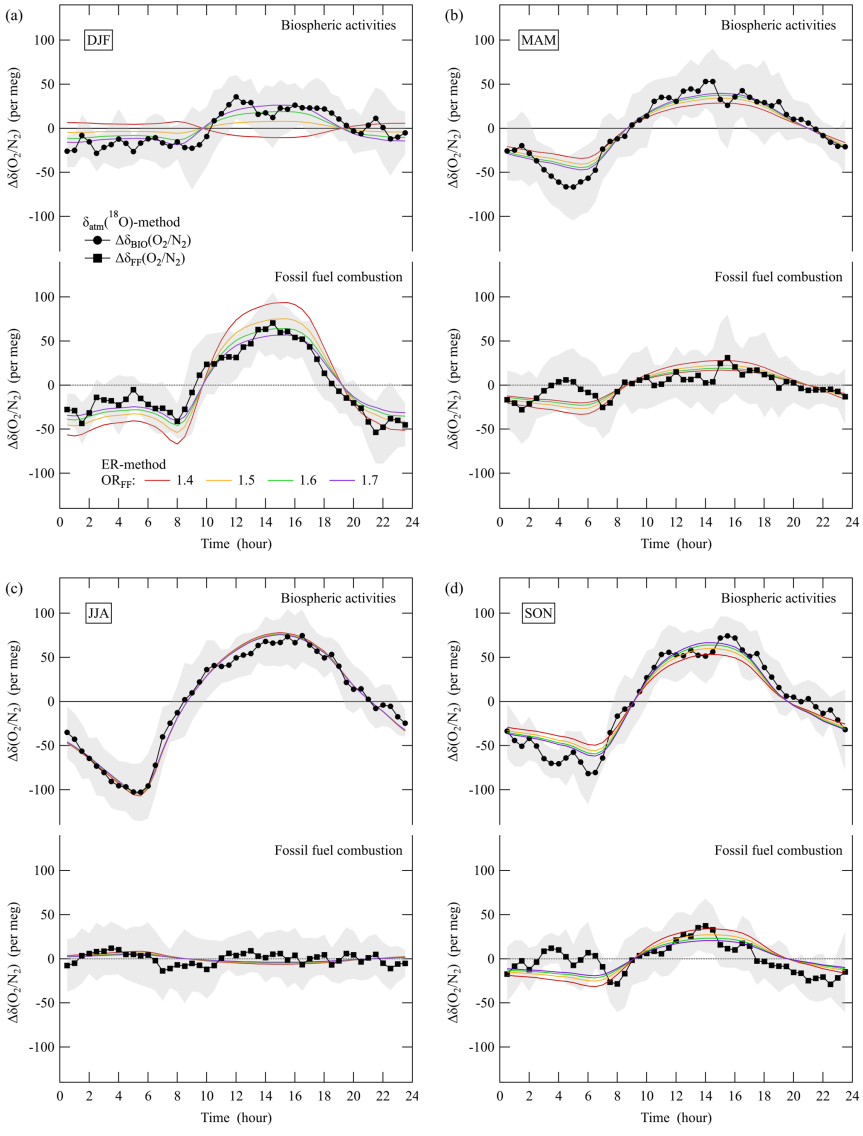

Figure 5: (a) Plots of average diurnal cycles of the $\Delta\delta_{BIO}(O_2/N_2)$ and $\Delta\delta_{FF}(O_2/N_2)$ for each season estimated by the $\delta_{atm}(^{18}O)$-method. $\Delta\delta(O_2/N_2)$ driven by activities in the terrestrial biosphere and fossil fuel combustion estimated by the ER-method are also shown.
670 **See text for details of the $\delta_{atm}(^{18}O)$- and ER-methods. Δ denotes deviations from the diurnal mean values. Error bands for $\Delta\delta_{BIO}(O_2/N_2)$ are derived from $\Delta\delta_{atm}(^{18}O)$ in Figure 4a. Error bands for $\Delta\delta_{FF}(O_2/N_2)$ are assumed to be the same as those for $\Delta\delta_{BIO}(O_2/N_2)$.**

https://doi.org/10.5194/egusphere-2024-654
Preprint. Discussion started: 3 April 2024

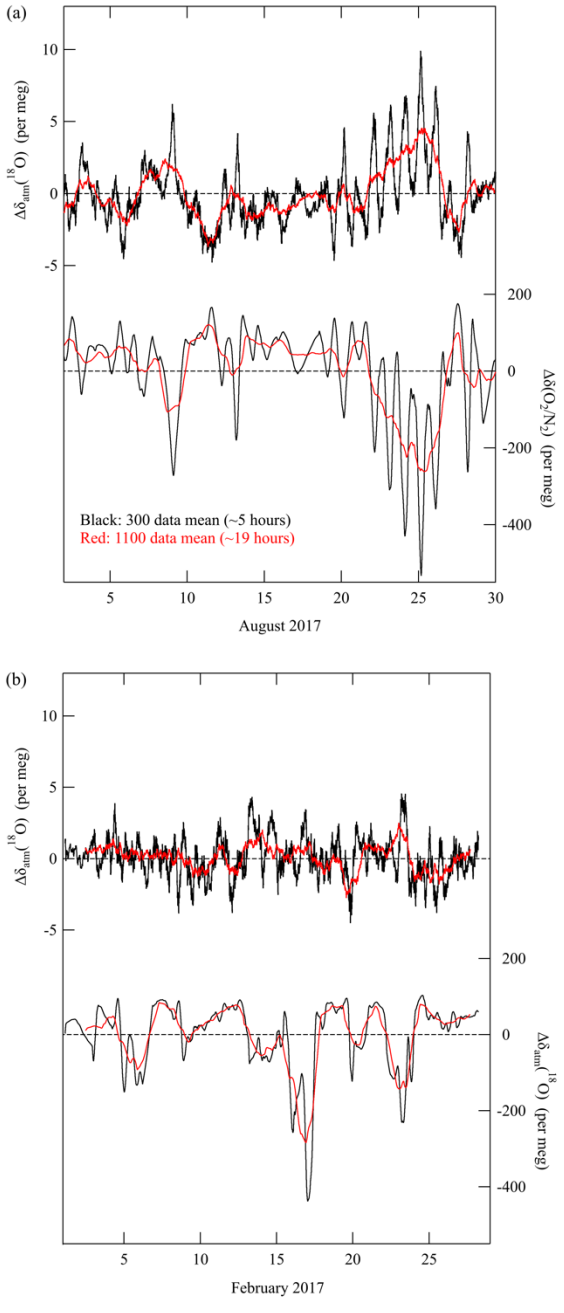

675

Figure 6: (a) Rolling average values of $\Delta\delta_{atm}(^{18}O)$ and $\Delta\delta(O_2/N_2)$ for 300 data (black) and 1100 data (red) at TKB in August 2017. Δ
680 **denotes deviations from the monthly mean value. (b) Same as in (a), but for February 2017.**

https://doi.org/10.5194/egusphere-2024-654
Preprint. Discussion started: 3 April 2024

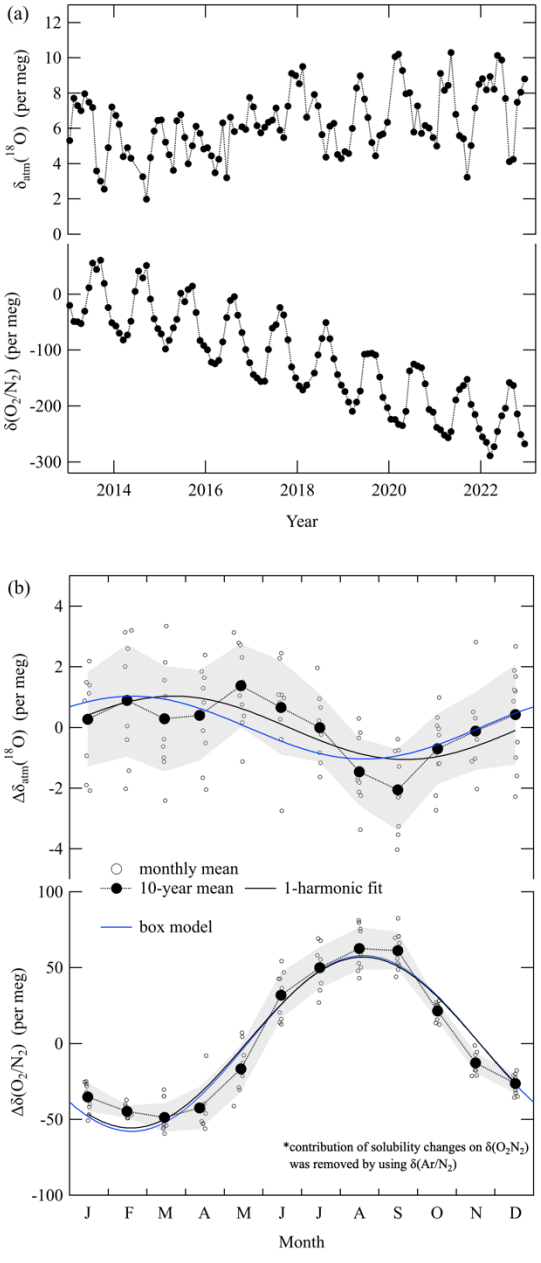

685

https://doi.org/10.5194/egusphere-2024-654
Preprint. Discussion started: 3 April 2024

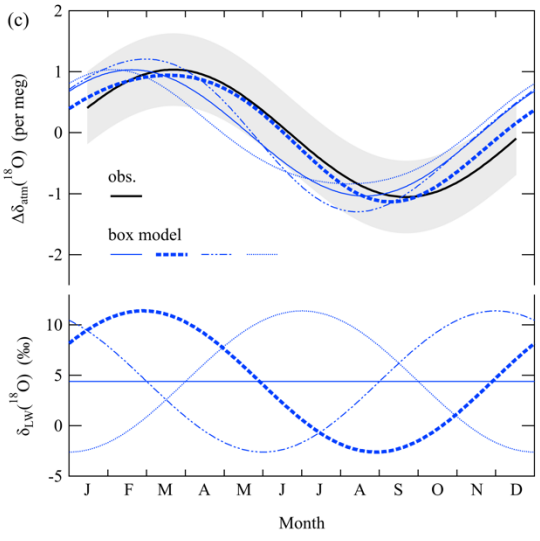

Figure 7: (a) Monthly mean values of $\delta_{atm}(^{18}O)$ and $\delta(O_2/N_2)$ observed at TKB for the period 2013–2022. Local effects of fossil fuel combustion around TKB were excluded from $\delta(O_2/N_2)$. See text for details. (b) Detrended monthly mean values (open black circles) and their 10-year average (filled black circles) of $\Delta\delta_{atm}(^{18}O)$ at TKB for the period 2013–2022. Those of $\Delta\delta(O_2/N_2)$, extracted by removing the contributions of solubility change by using the average seasonal $\delta(Ar/N_2)$ cycle at TKB (see text), are also shown. Average seasonal cycles of $\Delta\delta_{atm}(^{18}O)$ and $\Delta\delta(O_2/N_2)$ obtained by applying one-harmonic best-fit curves to the data (solid black lines) and those simulated by the box model (solid blue lines) are also shown. We assumed a constant $\delta_{LW}(^{18}O)$ of 4.4 ‰ for the simulation. Δ denotes deviations from the annual mean values. (c) Same best-fit curve for $\delta_{atm}(^{18}O)$ as in (b). Error bands indicate average deviations from the 10-year average of $\Delta\delta_{atm}(^{18}O)$ ($\pm1\sigma$). Same average seasonal cycle of $\Delta\delta_{atm}(^{18}O)$ simulated by a box model as in (b), and corresponding $\delta_{LW}(^{18}O)$ values (blue solid lines). Additional simulations of average seasonal $\Delta\delta_{atm}(^{18}O)$ cycles and the incorporated seasonally varying $\delta_{LW}(^{18}O)$ values are also shown (thick blue dashed, two-dot chain, and dotted lines).

https://doi.org/10.5194/egusphere-2024-654
Preprint. Discussion started: 3 April 2024

700

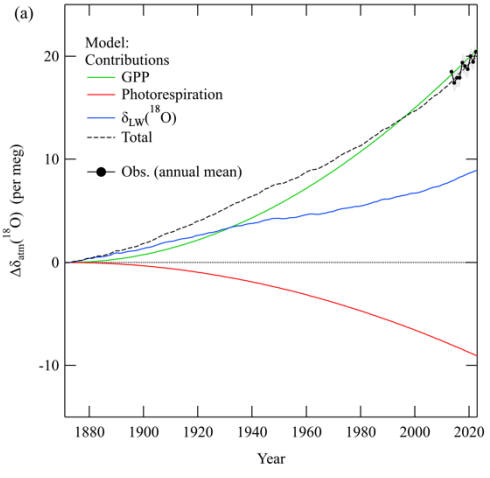

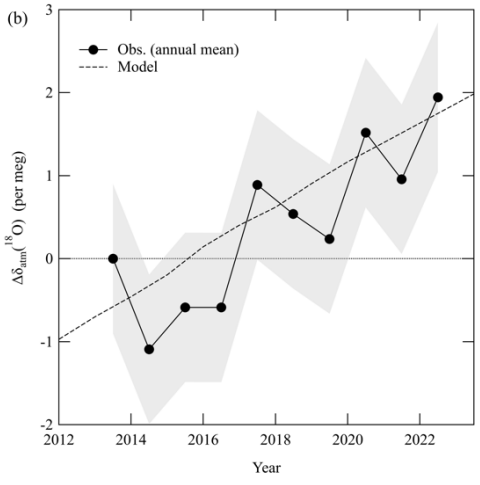

https://doi.org/10.5194/egusphere-2024-654
Preprint. Discussion started: 3 April 2024

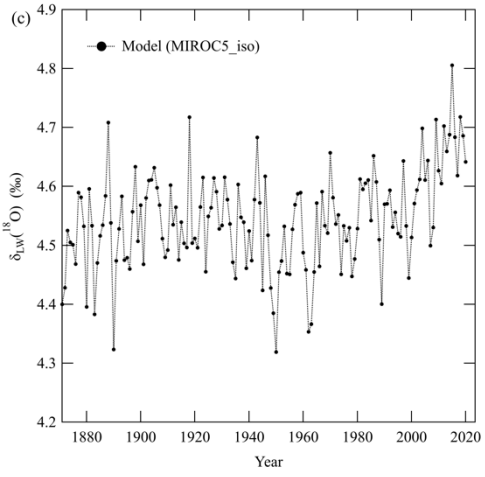

705

Figure 8: (a) Annual average values of $\Delta\delta_{atm}(^{18}O)$ observed at TKB (filled black circles). $\Delta\delta_{atm}(^{18}O)$ simulated by the box model for the period 1871–2022 (dashed black line) and the respective contributions of GPP (solid green line), photorespiration (solid red line), and $\delta_{LW}(^{18}O)$ (solid blue line) to the simulated $\delta_{atm}(^{18}O)$ are also shown (see text). Δ denotes deviations from the simulated value in 1871. (b) Same as in (b) but for data during 2012–2022. Δ denotes deviations from the observed value in 2013. (c) Annual average
710 **values of the global average $\delta_{LW}(^{18}O)$ calculated by MIROC5-iso. The value in 1871 was arbitrarily adjusted to 4.4 ‰.**